Detection of water vapour absorption around 363 nm in measured atmospheric absorption spectra and its effect on DOAS evaluations

Johannes Lampel[1,*], Denis Pöhler[2], Oleg L. Polyansky[3,4], Aleksandra A. Kyuberis[4], Nikolai F. Zobov[4], Jonathan Tennyson[3], Lorenzo Lodi[3], Udo Frieß[2], Yang Wang[1], Steffen Beirle[1], Ulrich Platt[2], and Thomas Wagner[1]

[1]Max Planck Institute for Chemistry, 55128 Mainz, Germany
[2]Institute of Environmental Physics, University of Heidelberg, 69120 Heidelberg, Germany
[3]Department of Physics and Astronomy, University College London, Gower St, London WC1E 6BT, UK
[4]Institute of Applied Physics, Russian Academy of Sciences, Nizhny Novgorod, Russia
[*]now at [2]

Correspondence to: J. Lampel (johannes.lampel@mpic.de)

Abstract.

Water vapour is known to absorb radiation from the microwave region to the blue part of the visible spectrum with decreasing efficiency. Ab-initio approaches to model individual absorption lines of the gaseous water molecule predict absorption lines up to its dissociation limit at 243 nm.

We present first evidence of water vapour absorption near 363 nm from field measurements using data from Multi-Axis differential optical absorption spectroscopy (MAX-DOAS) and Longpath (LP)-DOAS measurements. The identification of the absorptions was based on the recent *POKAZATEL* line list by Polyansky et al. (2016).

For MAX-DOAS measurements, we observed absorption by water vapour in an absorption band around 363 nm with optical depths of up to 2×10^{-3}. The retrieved column densities from two months of measurement data and more than 2000 individual observations at different latitudes correlate well with simultaneously measured well-established water vapour absorptions in the blue spectral range from 452-499 nm ($R^2 = 0.89$), but the line intensities at around 363 nm are underestimated by a factor of 2.6 ± 0.5 by the ab-initio model. At a spectral resolution of 0.5 nm, we derive a maximum cross-section value of 2.7×10^{-27} cm^2 molec^{-1} at 362.3 nm. The results were independent of the used literature absorption cross-section of the O$_4$ absorption, which overlays this water vapour absorption band.

Also water vapour absorption around 376 nm was identified. Below 360 nm no water vapour absorption above 1.4×10^{-26} cm^2 molec^{-1} was observed.

The newly found absorption can have a significant impact on the spectral retrievals of absorbing trace-gas species in the spectral range around 363 nm. Its effect on the spectral analysis of O$_4$, HONO and OClO is discussed.

1 Introduction

The most important greenhouse gas is water vapour. ~~it~~ It plays a key role ~~for~~ in the radiative balance of the Earth's atmosphere (e.g. Myhre et al., 2013). Due to the large temperature range covered by observations on Earth ~~, the upper atmosphere~~ but also

1
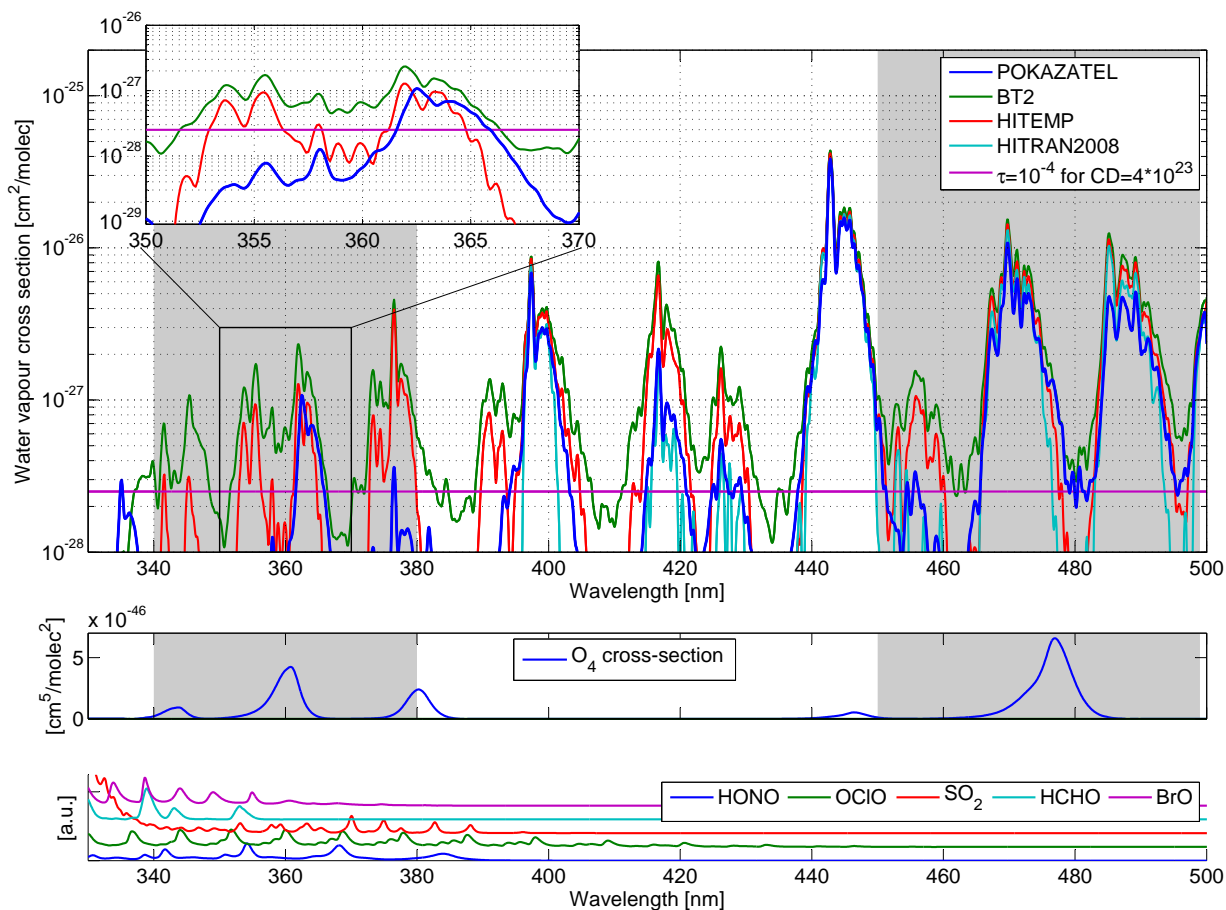
Figure 1. Overview of some recently published published water vapour cross-sections convoluted to a spectral resolution of 0.5 nm in the spectral interval from 330 to 500 nm. Also indicated is a typical MAX-DOAS detection limit for a differential OD of 10^{-4} at a water vapour column density of $4 \cdot 10^{23}$ molec cm^{-2} (purple line, top panel). The middle panels shows the O_4 absorption cross-section, the lowermost panel other absorbers of atmospheric relevance (HONO, OClO, SO_2, HCHO, and BrO) in this spectral range.

on exoplanets, and due to the spectral extend of observed water vapour absorption, accurate water vapour line lists covering different temperatures over a wide range of wavelengths are necessary. Since water vapour absorptions are present in many wavelength regions, precise knowledge of their properties is also required for assessing greenhouse effects. In addition it is required for spectroscopic detection of other trace gases, since their absorption structures often overlap with water vapour

5 absorption. The number of laboratory measurements of water vapour absorption spectra at different temperatures is limited due to technical reasons: Experimental measurements of water vapour absorption are not straightforward, as water vapour cannot be compressed to increase its optical depths in a measurement volume at any temperature. Moreover the absorption cross-section is relatively small in certain wavelength ranges, e.g. in the blue and near UV spectral ranges which concern us here. The gap between observed absorptions and the available literature absorption cross-sections from laboratory measurements

10 can be addressed by means of *ab initio* models for water vapour absorption lines, which can provide energy (i.e. wavelength), intensity, and additional parameters for each absorption line. This is done e.g. in the HITRAN database (Rothman et al., 2013), where information from measured absorption lines is merged with information from other sources such as *ab initio* models. In addition to HITRAN, other line list compilations are also available such as the GEISA database (Jacquinet-Husson et al., 2008), which lists water vapour absorption lines up to 25232 cm^{-1} (down to 396.3 nm).

15 Lampel et al. (2015b) found systematic structures in the fit residuals in this spectral range below 370 nm with magnitudes of around 5×10^{-4} in Multi-Axis Differential Optical Absorption Spectroscopy (MAX-DOAS) atmospheric observations, which could point towards a tropospheric absorber with absorption structures in this spectral range. The BT2 (Barber et al., 2006) and HITEMP (Rothman et al., 2010) line lists could explain some of the structures, but show inconsistencies. HITEMP is a synthesis of the 2008 edition of HITRAN Rothman et al. (2009) and BT2 with HITRAN lines replacing BT2 ones where

20 they were available [1]. Still, these two line lists show significant differences between each other, mostly due to the individual line cutoff employed in the HITEMP database (see also Figure 1). This cutoff removes weak absorption lines from the line list and was introduced for the HITRAN and HITEMP line lists to reduce the number of individual absorption lines for further processing as described e.g. in Rothman et al. (2010). It removes a large number of weak individual lines below the line intensity cutoff of $10^{-27} \text{ cm molec}^{-1}$ for wavelengths shorter than $1 \, \mu\text{m}$ (Rothman et al., 2010).

25 Polyansky et al. (2016) recently developed a computed line list (which we call *POKAZATEL* here, according to the first letters of the name of each author) containing water vapour lines in the spectral range below 400 nm. Prior to this publication, It is independent of the other sources and is based on a number of theoretical improvements compared to BT2. BT2 already listed absorptions in this spectral region were already listed in the computed line list prior to the publication of *POKAZATEL*. The *POKAZATEL* line list differs significantly from BT2 (Barber et al., 2006), on which HITEMP (Rothman et al., 2010) is

30 partly based. Howeverand thus also HITEMP below 380 nm (see Figure 1). In general, only a few of these absorption lines lines below 380 nm have also been reported from laboratory measurements (Dupré et al., 2005; Maksyutenko et al., 2012). For

---

[1]The HITRAN 2008, HITEMP and HITRAN 2012 data used here was downloaded from the HITRAN website (http://www.cfa.harvard.edu/hitran/) with the file name for HITRAN 2008 version 2009 "01 hit09.par", HITEMP "01 hitemp.par" and HITRAN 2012 "01 hit12.par". BT2 downloaded from the exomol project (Tennyson and Yurchenko, 2012) http://www.exomol.com/xsecs/1H2-16O

a compilation of spectroscopic data see Tennyson et al. (2013). Previous publications, such as HITRAN 2012 (Rothman et al., 2013)~~does not list absorptions~~, do not list water vapour lines below 388 nm.

Recently, Wilson et al. (2016) deduced upper limits for the water vapour absorption in the near-UV by incoherent broad-band cavity enhanced absorption spectroscopy (IBBCEAS) measurements in the laboratory. They estimated the water vapour absorption cross-section to be smaller than 5×10^{-26} cm^2 molec^{-1} at a spectral resolution of 0.5 nm between 340–420 nm. This is significantly smaller than the water vapour cross-section measured by Du et al. (2013) between 290–350 nm (see subsection 4.8).

~~Lampel et al. (2015b) found systematic residual structures in this spectral range below 370 nm with magnitudes of around 5×10^{-4} in Multi-Axis Differential Optical Absorption Spectroscopy (MAX-DOAS) atmospheric observations, which could point towards a tropospheric absorber with absorption structures in this spectral range. The BT2 and HITEMP line lists could explain some of the structures, but show inconsistencies. These two line lists show significant differences between each other, mostly due to the individual line cut-off employed in the HITEMP database (see also).~~

1.1 The 'POKAZATEL' line list

Following up on previous high quality computed water line lists (Partridge and Schwenke, 1997; Barber et al., 2006), the *POKAZATEL* line list (Polyansky et al., 2016) was calculated for the purpose of producing a complete list of water lines involving transitions between all the bound energy levels of $H_2{}^{16}O$ up to dissociation.

Until now the most complete water line list, called BT2 (Barber et al., 2006), only covered energy levels up to 30 000 cm^{-1} (333 nm) and rotational quantum numbers, J, up to 50. POKAZATEL covers the entire bound energies up to dissociation – 41 000 cm^{-1} (244 nm) (Boyarkin et al., 2013) and the highest J considered is 72.

POKAZATEL extends BT2 threefold. First, higher temperatures can be covered by the line list, as higher energy levels are involved and more hot transitions are calculated. Second, for room temperature the spectral range is expanded in the UV region down to ~~(in principle)~~ about 244 nm. Third, the predictions of the line positions and intensities by *POKAZATEL* should be considerably more accurate. In particular, POKAZATEL is based on variational nuclear motion calculations performed with the DVR3D program suite (Tennyson et al., 2004). In order to calculate the line positions and line intensities of the water lines two inputs into DVR3D are necessary – a water potential energy surface (PES) for the ground electronic state and a dipole moment surface (DMS). A global water PES, covering geometries up to dissociation, is available only from *ab initio* calculations (Császár et al., 2010) and is not accurate enough for our purposes. *POKAZATEL* is therefore based on the semi-empirical PES obtained by the fitting to the experimental data up to 41 000 cm^{-1} (Tennyson et al., 2013). The details of the fit are given by Polyansky et al. (2016). In particular, the RMS (root mean square) deviation for levels below 25 000 cm^{-1}, calculated by this fitted PES is about 0.03 cm^{-1} and the levels from 25 000 cm^{-1} to 41 000 cm^{-1} are reproduced to within about 0.1 cm^{-1} on average using measured data from Maksyutenko et al. (2007).

A very accurate, *ab initio*, global DMS was computed by Lodi et al. (2011) and was used without modification for the POKAZATEL line list calculation. This DMS has been used to successfully construct comprehensive line lists for $H_2{}^{17}O$ and $H_2{}^{18}O$ (Lodi and Tennyson, 2012) which were included in their entirety in the most recent, 2012, release of HITRAN. A recent

laboratory investigation has verified the accuracy of these line lists in the near-infrared (Regalia et al., 2014). However, as discussed below, the intensities predicted by the various line lists have yet to be validated in the near-uv.

1.2 ~~Potential impact~~ Impact on DOAS measurements of atmospheric trace gases

The absorption lines listed in the UV range in *POKAZATEL*, BT2 and HITEMP - which are to our knowledge presently not included in DOAS retrievals - could have an effect on the overall measurement errors of several trace-gas retrievals and could lead to systematic biases in the spectral evaluation of tropospheric absorbers in this spectral regions, such as ~~O_4, HONO, OClO and SO$_2$, potentially even HCHO and BrO~~ the oxygen dimer O_2-O_2 (or short: O_4), nitrous acid (HONO), chlorine dioxide (OClO) and sulphur dioxide (SO_2), formaldehyde (HCHO) and bromine monoxide (BrO). In subsection 4.11 we discuss these potential interferences. In **??** absorption cross-sections of these species are shown in the two lowermost panels.

In particular, spectral structures at around 360 nm have been observed in atmospheric DOAS measurements before and were either explained by erroneous ~~oxygen dimer O_2-O_2 (or in short: O_4)~~ O_4 literature cross-sections, e.g. an incorrect spectral calibration of the respectively used cross-section data (e.g. Wagner et al., 2002)~~, or~~. In any case, it could be possibly explained by an unaccounted tropospheric absorber. ~~lists a number of absorption lines which overlay the O_4 absorption at 360 nm. In cases where the absolute humidity during the measurement campaign does not change and therefore the correlation of the column densities determined from the absorptions of water vapour and O_4 is strong, as it is the case e.g. for the M91 campaign (see), it is difficult to disentangle the possible contribution of water vapour absorption and O_4 absorption.~~

1.3 Outline

Based on our field measurements combined with the *POKAZATEL* water vapour line list, which yields new information about water vapour absorption below 390nm, we make an attempt to answer the following questions:

1. Are the water vapour absorption bands near 335 nm, 363 nm and 376 nm found in atmospheric DOAS measurements?

2. Is the magnitude of these absorptions in agreement with measurements in other wavelength ranges? (compare also Lampel et al., 2015b, for the blue spectral range)

3. How well is the shape and the magnitude of the measured absorption bands reproduced by the line lists?

4. What are the consequences for the spectral retrieval of other trace-gases in the same spectral region ~~?~~ (as e.g. O_4, HONO and OClO)?

2 Atmospheric DOAS measurements

The data which was analysed here was collected during three different field campaigns, where different DOAS instruments were used.

1. MAX-DOAS data from cruises *ANT XXVIII/1-2* (Naggar, 2012; Kattner, 2012) of the research vessel 'Polarstern', which covered latitudes from 54°N (northern Germany) to 70°S (coastal Antarctica).

2. MAX-DOAS data from the 'Surface Ocean PRocesses in the ANtropocene' (SOPRAN) cruise M91 with the research vessel 'Meteor' in the Peruvian upwelling region in December 2012 (Bange, 2013).

3. Longpath (LP)-DOAS Measurements were analysed for water vapour using data from a dedicated measurement period in Heidelberg in August and September 2015 (further called *HD15*).

Both MAX-DOAS cruises were largely unaffected by anthropogenic pollution, which avoids interferences of high NO$_2$ absorption structures in the data evaluation.

~~The MAX-DOAS measurements during the M91 campaign were performed at a spectral resolution of 0.45 nm, but due to the limited latitudinal~~ Due to the small latitudinal and temporal extent of the cruise ~~track~~ M91 (compare Table 1 and Figure 2), the variation of water vapour volume mixing ratios (VMR) was small. The VMR was, according to the meteorological station onboard, between 1.6 – 2.4%. Therefore observed differential column densities (dSCDs, section 3) of H$_2$O and O$_4$ correlate well due to changes in the effective light path lengths and cannot be unambiguously disentangled. In a first order approximation, the O$_4$ dSCD is proportional to the effective light path length, the H$_2$O dSCD is proportional to the light path length as well, but also to the absolute humidity along the light path (Equation 2). The campaign *ANT XXVIII/1-2* took place along a cruise track from Bremerhaven/Germany to Antarctica~~and therefore~~. It allows to distinguish actual water vapour absorption from systematic errors ~~in the O$_4$ cross-sections employed~~of other trace gases, such as the absorption of O$_4$. Water vapour VMR were found between 0.5 – 3.0% according to the meteorological station onboard. The MAX-DOAS instrument onboard Polarstern has a lower spectral resolution of 0.7 nm (UV) and 0.9 nm (VIS)~~, but~~. It has the advantage of a wider spectral range allowing for independent simultaneous observations of H$_2$O and O$_4$ at around 361 nm and 477 nm due to the spectral overlap of both absorbers (compare **??**).

Dedicated LP-DOAS measurements were performed in Heidelberg in August and September 2015. The advantage is the high spectral resolution of 0.2 nm and the well-defined light-path of these active measurements. However, high NO$_2$ concentrations can cause spectral interferences and the range of absolute water vapour volume mixing ratios (VMR) is relatively limited (see subsection 4.1).

3 The DOAS Method

The DOAS (Differential Optical Absorption Spectroscopy) method (Platt and Stutz, 2008) relies on attenuation of light with a wavelength λ from suitable light sources (intensity I_0) by absorbers within the light path according to Lambert-Beer's law $I(\lambda) = I_0(\lambda) \cdot \exp(-\tau(\lambda))$. The optical density (OD) $\tau(\lambda)$ is calculated from a reference spectrum $I_0(\lambda)$ and a measurement spectrum $I(\lambda)$, $\tau(\lambda) = -\ln \frac{I(\lambda)}{I_0(\lambda)}$. ~~To be independent of~~ The measured OD of the broad-band extinction and scattering by molecules and particles ~~, the measured OD is partly compensated~~ is represented by a broad-band polynomial $p(\lambda)$~~or~~. Or the measured OD is filtered into a broad-band and a narrow-band contribution. Characteristic ~~and narrow-band~~ absorption
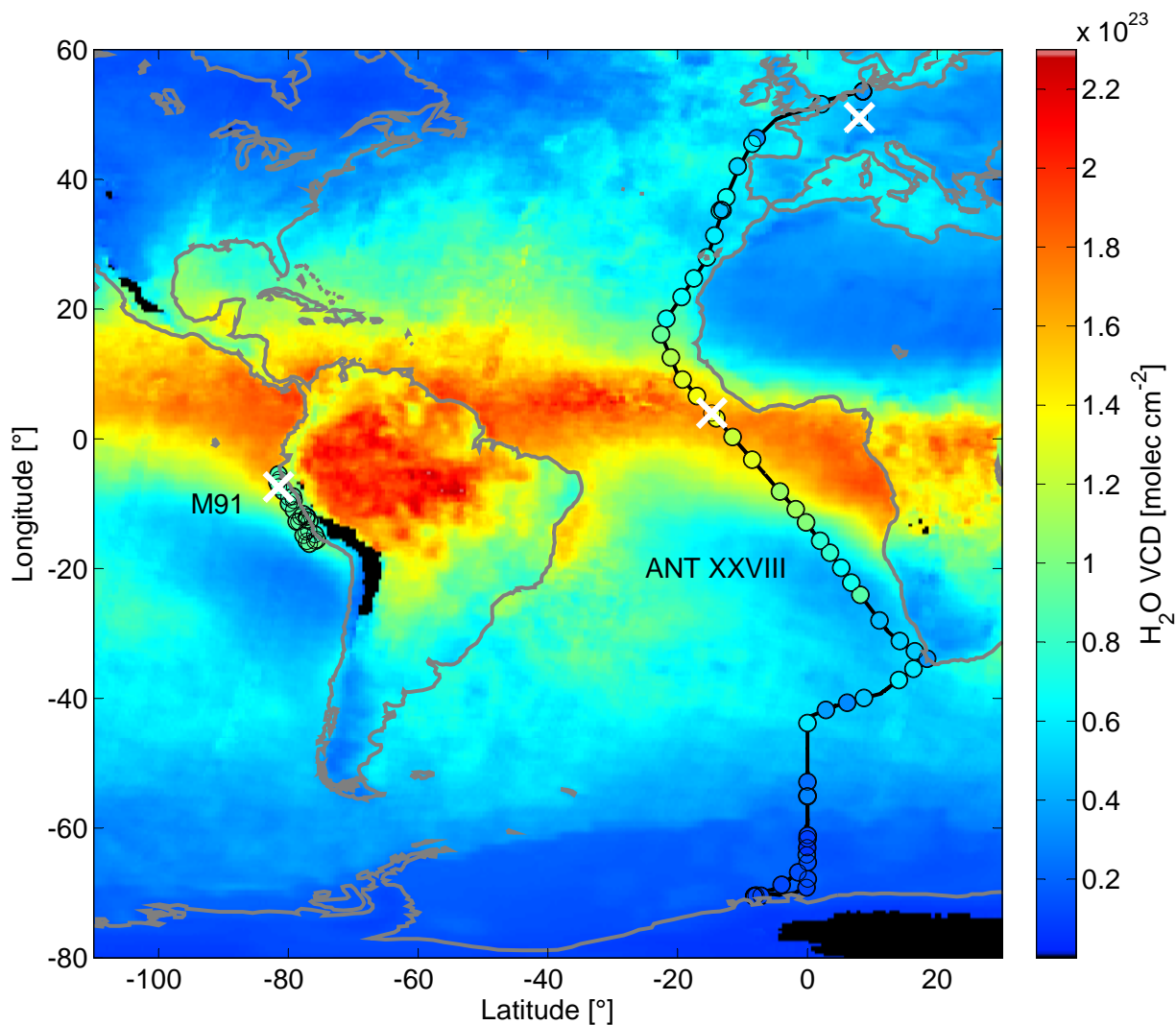
Figure 2. Measurement Overview: The cruise track of M91 (Peruvian Upwelling) and *ANT XXVIII/1-2* (Atlantic) is shown, additionally the location of the LP-DOAS measurements in Heidelberg, Germany is marked (white cross in the north-east corner of the map). The background shows GOME-2A H_2O VCDs (Wagner et al., 2003) averaged from November and December 2011 (time during *ANT XXVIII/1-2*). The locations of the measurements shown in Figure 3 and Figure 5 are also marked by white crosses. Daily error-weighted averages of H_2O/O_4 dSCD ratios (measured in the wavelength range from 340-380 nm at 3° telescope elevation, corrected according to Figure 6) are shown as circles and converted to a VCD assuming an exponential water vapour concentration profile with a scale height of 2 km.

Name	Type	Location, Time	Spec. range [nm]	Spec. resolution [nm]	Spectrograph (focal length)	H$_2$O VMR %
~~ANT XXVIII~~ *ANT XXVIII/1-2*	MAX-DOAS	Atlantic 54°N - 70°S October - December 2011	277-413 390-617	0.7 0.9	OMT f=60 mm	0.5–3.0
M91	MAX-DOAS	Peru, coastal upwelling 5°S 82°W–16°S 75° W December 1st–25th 2012	324-467	0.45	Acton 300i f=300 mm	1.6–2.4
HD15	LP-DOAS	Heidelberg 49°25'N 8°43'W August+September 2015	329–371 426–465	0.2 0.2	Acton 300i f=300 mm	0.4–1.3

Table 1. Campaigns of which measurements were used. The cruise tracks of the ship-borne MAX-DOAS measurements are shown in Figure 2.

features of different absorbing trace-gas species with the total cross-section $\sigma_i(\lambda)$ are then used to determine their respective concentrations $c_i(l)$ along the light path L:

$$\tau(\lambda) = \sum_i \sigma_i(\lambda) \int_0^L c_i(l)dl + p(\lambda) \tag{1}$$

The column density $S_i = \int_0^L c_i(l)dl$ is calculated by a fitting routine, which is applied to data from a given wavelength
5 interval with a width of several nm to several 10 nm. The absorption path L is known for LP-DOAS measurements and can be estimated or calculated from radiative transfer models for MAX-DOAS measurements. The high resolution literature cross-sections $\sigma_{L,i}$ are convoluted with the measured instrument function H of the respective setup to obtain $\sigma_i = H \otimes \sigma_{L,i}$, the absorption cross-section as it would be determined by the instrument. The instrument slit function is usually measured by observing individual atomic emission lines of mercury, which have a spectral width which is two orders of magnitude smaller
10 than the resolution of the instrument (Sansonetti et al., 1996).

LP-DOAS measurements (subsection 3.1) have the advantage of a well-defined light-path and the possibility of measurements at night, but typically do not yield as small ~~residuals~~ measurement errors of SCDs as MAX-DOAS (subsection 3.2) observations. The disadvantage of MAX-DOAS measurements is ~~,~~ that their effective light-path length depends on

various factors such as atmospheric state (aerosols, clouds), which is often not known precisely. This needs to be explicitly considered in the data evaluation (subsection 4.2).

3.1 LP-DOAS Measurements

~~A description of the LP-DOAS instrument used here can be found in **?** and Eger (2014). The total light path used for the measurements reported was 6.12 km long: Above the city of Heidelberg from the roof of the Institute of Environmental Physics to retro-reflectors mounted at the train station 'Molkenkur'. The spectral resolution was 0.2 nm in both spectral ranges.~~

The Longpath(LP)-DOAS instrument is based on an artificial light source (here a ~~a~~ LASER-driven light source Energetiq LDLS-EQ-99), retro reflectors, a telescope and a spectrometer. The light is sent by a telescope across the measurement distance to a retro reflector, which reflects the light back onto the same telescope. It collects the received light and transfers it to a spectrograph. A ~~sequence of~~ measurement sequence consists of four spectra: actual measurement spectra, light-source spectrum measurements without absorption and the respective background measurements (i.e. measurements with the light source switched off or blocked)~~, light-source spectrum measurements without absorption and actual measurement spectra is used to ensure~~ . The correction of the measurement spectra with background spectra ensures independence of the measured spectra from external sunlight and instrumental instabilities ~~(?). The~~ (Pöhler et al., 2010).

A description of the LP-DOAS ~~setup has the advantage that the actual light path is well-defined and thus average concentrations of absorbing molecules can be directly derived, also measurements at night are possible.~~ instrument used here can be found in Pöhler et al. (2010) and Eger (2014). The total light path used for the measurements reported was 6.12 km long: Above the city of Heidelberg from the roof of the Institute of Environmental Physics to retro-reflectors mounted at the train station 'Molkenkur' and back to the institute.

The optical density $\tau(\lambda)$ is calculated from a background corrected light source spectrum and a background corrected atmospheric spectrum and filtered by a binomial high-pass with 1000 iterations. The convoluted and high-pass filtered literature cross-sections listed in Table 2 are then fitted in the respective fitting interval to the corrected OD.

3.2 MAX-DOAS Measurements

Hönninger and Platt (2002) described the method of Multi-Axis DOAS (MAX-DOAS) measurements which improve the sensitivity of passive DOAS observations at altitude ranges close to the instrument (i.e. up to a few km). It uses scattered sunlight collected by a telescope pointing towards the sky at different elevation angles α. The horizon is here defined as $\alpha = 0°$, zenith viewing direction as $\alpha = 90°$. Each elevation has a different sensitivity for absorptions in different heights of the atmosphere. Low elevation angles have a higher sensitivity to absorbers close to the surface, because the additional light path compared to a zenith spectrum recorded at the same time and location is mostly located within the lowermost layers of the atmosphere (Hönninger et al., 2004).

9

	T [K]	MAX-DOAS					LP-DOAS		
		O$_4$/H$_2$O	O$_4$/H$_2$O	HONO	BrO	OClO	H$_2$O	H$_2$O	
Wavelength interval [nm]	Start	340	452	337	332	332	356	441	
	End	380	499	375	358	370	370	450	
H$_2$O vapour	298		×					×	HITEMP (Rothman et al., 2010)
		×		×	×	×	×		Polyansky et al. (2016)
O$_4$	293	×	×	×	×	×	×	×	Thalman and Volkamer (2013)
	273	(×)					(×)		
	203	(×)							
	287	(×)							Hermans et al. (2003)
	296	(×)							Greenblatt et al. (1990)
O$_3$	223	×	×	×	×	×			Serdyuchenko et al. (2014)
	243			×	×	×			
	293						×		
HCHO		×		×	×	×	×		Chance and Orphal (2011)
HONO				×		×			Stutz et al. (1999)
BrO		×		×	×	×			Fleischmann (2004)
OClO						×			Bogumil et al. (2003)
SO$_2$				(×)					Vandaele et al. (2009)
NO$_2$	293	×	×	×	×	×	(×)		Vandaele et al. (1998)
NO$_2$	293						×	×	Voigt et al. (2001)
NO$_2$ absorption cell	293K						(×)		
Ring Spectrum at	273K	×	×	×	×	×			DOASIS (Kraus, 2006)
	243K	×		×	×	×			which uses Bussemer (1993)
Ring Spectrum ·λ^4		×	×	×	×				Wagner et al. (2009)
Polynomial degree		3	3	5	3	4	3	3	
Add. Polynomial degree		1	1	1	1	1	0	0	

Table 2. Retrieval wavelength intervals and reference spectra for the MAX-DOAS and LP-DOAS measurements. Literature cross-sections listed in brackets were used for sensitivity studies.

The slant column density (SCD) is defined as the integral over the concentration ρ c_i along the light path L and is hence given in units of *molecules cm^{-2}*.

$$S = \int_L \rho(s)ds \,_L c_i(s)ds \tag{2}$$

From MAX-DOAS measurements differential slant column densities (dSCDs) can be calculated for each fitted trace gas: A so-called Fraunhofer reference spectrum (we follow the customary nomenclature to call such a spectrum Fraunhofer spectrum although it also contains spectral features from Earth's atmosphere) $I_0(\lambda)$ is chosen from one of the measurement spectra and the $\mathrm{dSCD}(\alpha) = \mathrm{SCD}(\alpha) - \mathrm{SCD}_{ref}$ is obtained from the DOAS fit for each elevation angle α relative to the Fraunhofer reference. ~~Typically a zenith spectrum is taken as reference and thus $\mathrm{SCD}_{ref} = \mathrm{SCD}(90°)$~~ In the measurements reported here, the DOAS fit includes the cross-sections listed in Table 2. By choosing references recorded shortly before and after the measurement spectrum the influence of ~~the~~ instrumental instabilities on the result was minimized as well as the influence of stratospheric absorbers.

3.2.1 The MAX-DOAS instrument during *ANT XXVIII/1-2*

The MAX-DOAS instrument operated during Polarstern cruise *ANT XXVIII/1-2* consists of a telescope unit mounted on the deck of Polarstern at port-side, which actively corrects for the roll movement of the ship, and a spectrometer unit with two temperature stabilized OMT spectrometers (f=60 mm, $|\Delta T| < 0.1°\mathrm{C}$, $\Delta\lambda < 0.01\,nm$), which had both been modified to minimize instrumental stray light (Lampel, 2014). Both spectrometers use back-thinned and peltier-cooled Hamamatsu S10141 CCD-detectors in order to have a high quantum efficiency in the UV range. The optical resolution of the instrument during this campaign was 0.7 nm and 0.9 nm and it covered a spectral range from 277–413 nm and 390–617 nm, respectively. Spectra were recorded for two minutes each at 7 elevation angles of 90° (zenith), 40, 20, 10, 5, 3, 1°, respectively, as long as solar zenith angles (SZA) were below $85°$. Glyoxal data from this campaign was published in Mahajan et al. (2014).

3.2.2 The MAX-DOAS Instrument during M91

A description of the instrument operated during SOPRAN cruise M91 can be found in Großmann et al. (2013). The optical resolution of the instrument during this campaign was 0.45 nm~~and it~~. It covered a spectral range from 324 nm to 467 nm. The telescope elevation control unit actively compensated the ship's roll movement. Spectra were recorded for one minute each at 8 elevation angles of 90° (zenith), 40, 20, 10, 6, 4, 2, 1°, respectively, as long as solar zenith angles (SZA) were $\leq 85°$.

3.3 Spectral retrieval (MAX-DOAS)

The fit settings are summarized in Table 2, example fits are shown in Figure 5. As Fraunhofer reference spectra the sum of the two 40° elevation angle spectra closest in time were used. Spectra recorded at a telescope elevation of 90° were not used as reference spectra, since they could have been influenced by direct sunlight during each of the MAX-DOAS campaigns close to the equator. The wavelength calibration was performed using recorded mercury discharge lamp spectra. On *ANT XXVIII/1-2*

11

these were recorded automatically each night together with offset and dark-current spectra, during M91 they were recorded manually.

~~Measurement errors~~ An additional intensity offset polynomial was used in the spectral evaluation to compensate for instrumental stray light, as described e.g. in (Peters et al., 2014).

5   Measurement errors of dSCDs are calculated as twice the DOAS fit error, according to Stutz and Platt (1996). This estimate is justified, because the standard deviation of the residual of the linear fit of H_2O/O_4 ratios at 363 and 477nm shown in Figure 6 amounts to 2.1 times the average DOAS fit error and the residual spectra from the DOAS fit are dominated by noise in the UV. This estimate disregards possible systematic errors, but these are estimated to be small compared to the water vapour absorption ($< 2 \times 10^{-4}$) as the residual spectra are dominated by random noise (see Figure 5).

10 For the water vapour absorption near 363nm, the wavelength interval was chosen using the technique described in Vogel et al. (2013) on spectra recorded on one individual day (November 15th, 2011 at about 6°N and 17°W) of the *ANT XXVIII/1-2* data set using the O_4 cross-section at 298K by Thalman and Volkamer (2013): For narrower wavelength ranges beginning above 345 nm and ending below 375 nm lower H_2O dSCDs were observed during the day. However the standard deviations of the H_2O dSCDs for these retrieval intervals are with $5 - 6 \times 10^{23}$ molec cm^{-2} (uncorrected) as large as the mean dSCDs. For the

15 larger fit intervals the standard deviation is significantly smaller ($1 - 2 \times 10^{23}$ molec cm^{-2}) and the ratio of standard deviation of H_2O dSCDs and the average fit error is close to 2, as expected from Stutz and Platt (1996). For the broader fit intervals the H_2O dSCD varies for fit intervals within 330-390 nm with a standard deviation of 16% of mean H_2O dSCD. We thus estimate the error due to the choice of fit settings to be below 20%. We assume that the small absorption structures of BrO and HCHO, which are not sufficiently constrained within fit intervals beginning above 345 nm cause this effect and/or possible

20 compensation of the relatively broad O_4 absorption by the DOAS polynomial. When including HONO in the DOAS analysis for this day with low NO_2 concentrations and thus presumably low HONO concentrations, enhanced HONO and H_2O dSCDs are observed simultaneously for fit intervals ending above 382 nm.

3.3.1 The blue spectral range

The effective center of the respective absorptions of O_4 and H_2O can be calculated for each fit interval $[\lambda_1, \lambda_2]$ using

25
$$\lambda_m = \frac{1}{\int_{\lambda_1}^{\lambda_2} \sigma(\lambda) \mathrm{d}\lambda} \int_{\lambda_1}^{\lambda_2} \lambda \times \sigma(\lambda) \mathrm{d}\lambda \quad \lambda \sigma(\lambda) \mathrm{d}\lambda \tag{3}$$

In the wavelength interval from 452-499 nm, the effective center of the water vapour absorptions of $\lambda_m^{H_2O} = 479$ nm is close to the effective center of the O_4 absorptions at $\lambda_m^{O_4} = 476$ nm.

The fit range was chosen to have similar effective centers of absorptions of O_4 and H_2O in order to have comparable conditions for radiative transfer at both wavelengths.

30 HITEMP was chosen for the water vapour absorption cross-section in the blue wavelength region. The differences in the blue wavelength region to HITRAN 2012 are negligible at a spectral resolution of 0.5 nm. HITEMP was chosen instead of POKAZATEL in the blue wavelength range, as already a couple of previous publications use this cross-section in the blue

wavelength range (see e.g. Lampel et al., 2015b, and references therein). As described in subsection 4.12 better agreement with observations was found for HITEMP than for POKAZATEL from 452-499 nm.

3.3.2 The near-UV spectral range

In the analyzed wavelength interval of 340-380 nm the absorption structures of O_4 and H_2O are centered around $\lambda_m^{O_4} = 361$ nm and $\lambda_m^{H_2O} = 364$ nm.

As the observed optical depth (OD) in the fit ranges around 360 nm are small, except for the absorption of O_4 and the OD related to the Ring effect, it was necessary to include in addition to the normal Ring spectrum the temperature dependence of the Ring spectrum. ~~This~~ The Ring spectrum itself compensates the measured apparent optical density due to inelastic scattering of sunlight at air molecules (Shefov, 1959; Grainger and Ring, 1962), which leads to an effective filling-in of Fraunhofer lines in the measured spectrum of scattered sunlight (e.g. Wagner et al., 2009, and references therein). The temperature dependence originates from the temperature dependence of the population of rotational states of the air molecules. It was calculated from the difference of Ring spectra $R(T)$ calculated at T=273 K and T=243 K using DOASIS (which is based on the work from Bussemer (1993), parts of which can also be found in Platt and Stutz (2008)): $\Delta R/\Delta T = (R(T - \Delta T) - R(T))/\Delta T$. The ~~temperature dependence of the~~ OD associated with the Ring spectrum temperature dependence amounts to up to 5×10^{-4} for the M91 data set when using a Ring spectrum calculated at 273K. For a Ring signal of 2.5×10^{25} molec cm^{-2} (which is typical for MAX-DOAS observations), the temperature effect of the Ring effect results in an OD of 5×10^{-4} for a temperature difference of 30 K. We found that warmer effective Ring temperatures were found at low telescope elevation angles, which agrees with the lower tropospheric temperature height profile. The temperature dependence of the derivative of the Ring spectrum with respect to temperature ~~is~~ was found to be smaller than 0.5% / 1K, therefore it was sufficient to use one individual spectrum to linearise this effect. ~~The OD associated with the Ring spectrum temperature dependence amounts to up to 5×10^{-4} for the M91 data set when using a Ring spectrum calculated at 273K.~~

The contribution of vibrational Raman scattering of air on measurements in this spectral range could be correlated to the size of the Ring effect and agreed in its magnitude with the calculations given in Lampel et al. (2015a). Its effect on the results presented here was however neglible and was only consistently observed when co-adding spectra from more than 4 elevation sequences and for RMS of the resulting residuals of less than 1×10^{-4}. The effect of the wavelength dependence of the AMF for the O_4 absorptions at 344, 361 and 380 nm was found to be negligible for the spectral retrieval of water vapour absorption in this spectral range.

4   Results and Discussion

Starting with the largest absorption band below 380 nm listed in *POKAZATEL* at around 363 nm, we show first experimental evidence of water vapour absorption in the UV from LP-DOAS measurements (subsection 4.1), which have the advantage of a well-defined light path length. These are complemented by even clearer detection of this absorption band by MAX-DOAS observations (subsection 4.2). The magnitude of the absorption is quantified by comparison to water vapour absorption in the

blue spectral range. From these results based on MAX-DOAS observations, a correction of the strength of the water vapour absorption band listed in *POKAZATEL* is derived.

We then also estimated the magnitude of the weaker water vapour absorption bands at 335nm (subsection 4.6) and 373 nm (subsection 4.7).

5   4.1   LP-DOAS: Detection of water vapour absorption at 363 nm

Measurements between 22 August and 24 September, 2015 were used for this analysis—, when optimal instrumental performance could be guaranteed. Measurement spectra were co-added in order to reduce the RMS of the residual in the UV fit interval to values of $1.5 \pm 0.3 \times 10^{-4}$ along the total light path of 6.12 km, which resulted in a time resolution of two hours. This corresponds to an exposure time of about 15 minutes for each measurement spectrum. Due to the need to change

10   the wavelength setting of the spectrometer between the different spectral windows around 440nm and 360nm, the time for each measurement sequence is shorter than the total time resolution.
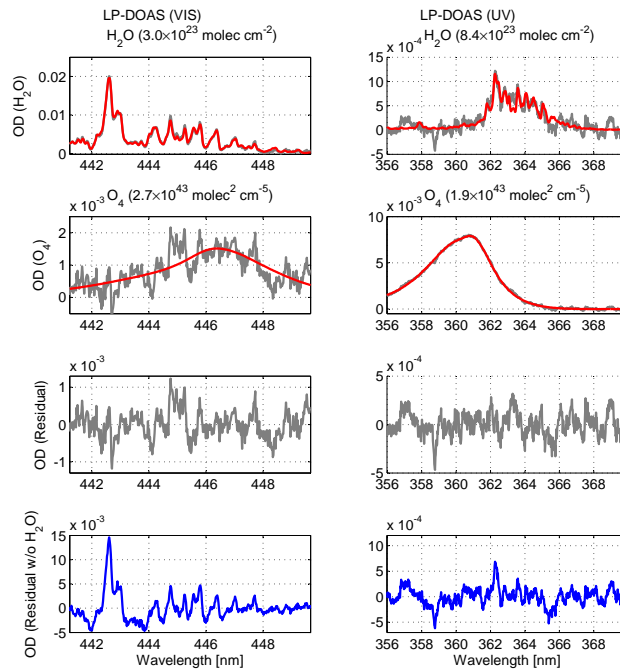
Figure 3. A LP-DOAS fit result for the fitting intervals around 363 and 442 nm. The spectra were recorded on August 29th, 2015 between 20:58 and 21:45 UTC. Top left panel: At 442 nm the H_2O dSCD $(3.0 \pm 0.04) \times 10^{23}$ molec cm^{-2} (O_4 dSCD $(2.7 \pm 0.6) \times 10^{43}$ molec^2 cm^{-5}). Top right panel: At 360 nm the H_2O dSCD $(8.4 \pm 0.6) \times 10^{23}$ molec cm^{-2} (O_4 dSCD $(1.85 \pm 0.03) \times 10^{43}$ molec^2 cm^{-5}).

A weak correlation of the water vapour absorption around 363 nm to the absorption at 442 nm was found with a correlation coefficient of $R^2 = 0.25$ (Figure 4) for individual measurements. The rather weak correlation is due to the large individual
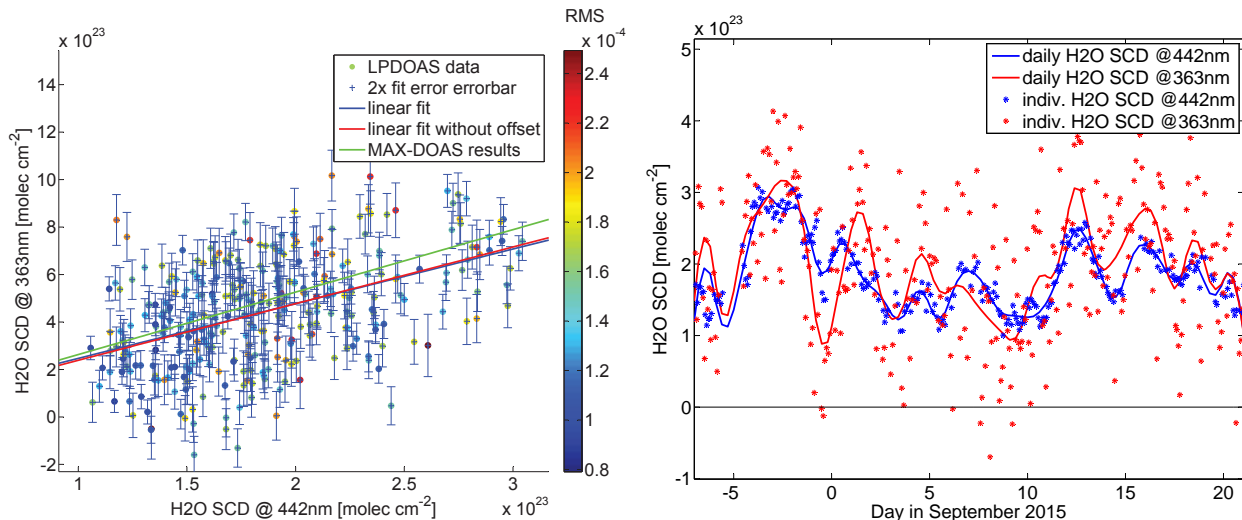
Figure 4. Left: Correlation of H_2O SCDs from LP-DOAS measurements near 363 and 442 nm. Also shown is the result from Table 3 line (1) from MAX-DOAS observations. **Right:** Time series of H_2O column densities from LP-DOAS measurements near 363 and 442 nm. Values near 363 nm were corrected by the scaling factor 2.31 ± 0.25 determined from the correlation plot on the left.

measurement errors~~, which~~. This can be directly seen by the large variations from one measurement to the next in the time series shown in Figure 4 on the right. For daily averaged values the correlation amounts to $R^2 = 0.61$. Further co-adding of spectral measurement data could not reduce the measurement errors further, as systematic residual structures appear (see Figure 3). Furthermore large NO_2 concentrations of up to 20 ppb led to additional residual structures. Selecting measurement spectra according to the NO_2 concentration or RMS did not improve the correlation.

As the measurement period was in late summer with temperatures between 9–36°C and relative humidity between 20–96% leading to a water vapour VMR between 0.4-1.3% (5–16.5 g m^{-3}), low as well as high VMRs are not well represented in this data set. This increases the error in the correlation of water vapour column densities determined in both wavelength intervals (see Table 2). Linear regression yields a relative magnitude of the absorption near 363 nm of 2.31 ± 0.25 and an offset of $1.6 \pm 4.5 \times 10^{22}$ molec cm^{-2}. Fixing the offset to zero yields a scaling factor for the absorption cross-section near 363 nm of 2.39 ± 0.05. This means, the *POKAZATEL* line lists underestimates the observed absorptions near 363 nm by a factor of ~~2.39 ± 0.05~~2.39. The measurement error will contribute significantly to the error of the scaling factor, as it is about 30% of the maximally measured column density near 363 nm. Thus we estimate the overall scaling factor from LP-DOAS measurements to be 2.4 ± 0.7.

4.2 MAX-DOAS: Detection of water vapour absorption near 363 nm

The absorption of water vapour was detected at about 363 nm (27548 cm^{-1}) in measurements from *ANT XXVIII/1-2* and M91, using a fit interval from 340-380 nm (26316-27548 cm^{-1}) according to Table 2. The maximum signal-to noise ratio dur-

ing both cruises (ratio between fitted H_2O dSCD and measurement error) were 14 and 10, respectively (15 and 20, respectively, for 16 co-added elevation sequences). The corresponding dSCD values showed the typical separation for each elevation angle as observed for water vapour absorptions in the blue wavelength range. The corresponding spectra are shown in Figure 5.
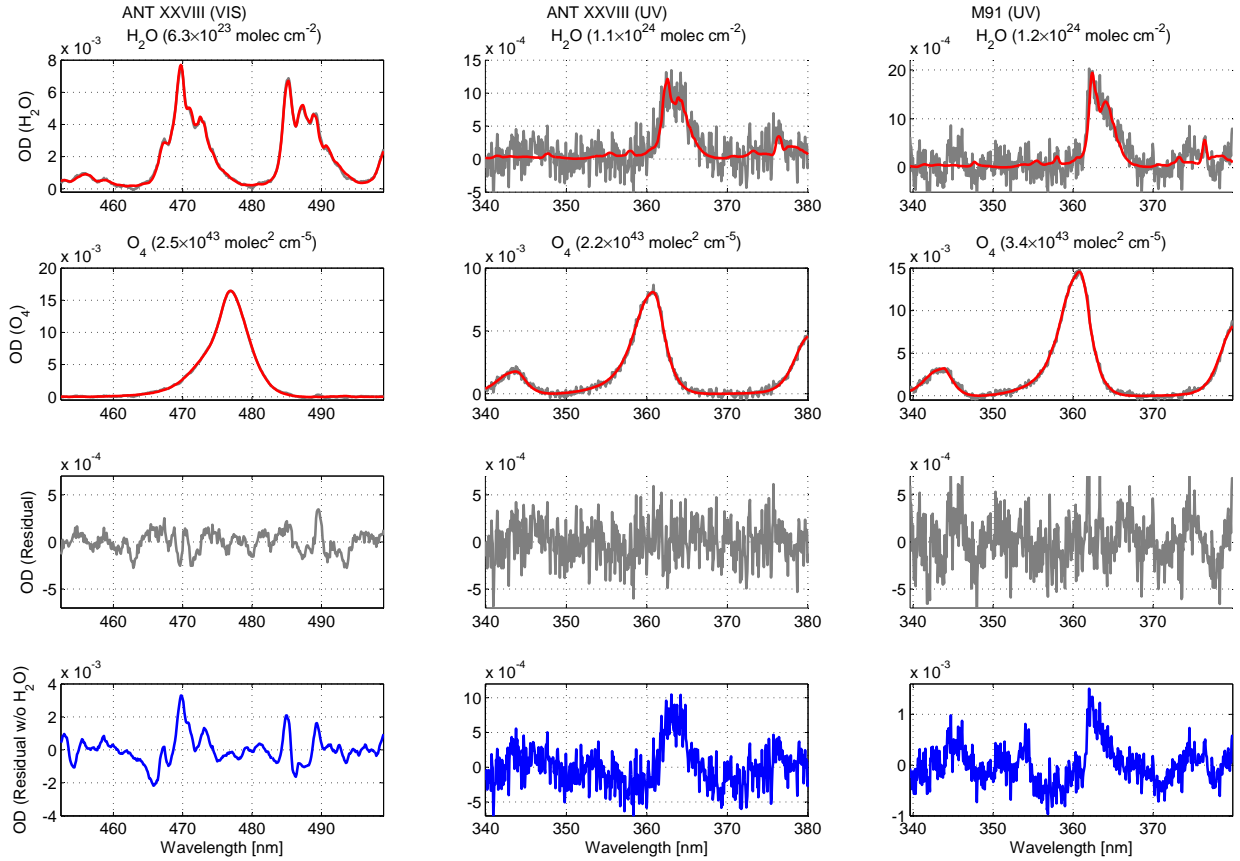
Figure 5. Fit results from *ANT XXVIII/1-2* and M91 showing the detection of water vapour absorptions at 477 nm and 363 nm; in red, the modeled absorptions according to the cross-sections listed in Table 2, in grey, the measured values. In blue, the residual is shown if no water vapour absorption was included in the fit. The fits from *ANT XXVIII/1-2* use a spectrum (exposure time: 120 s, spectral resolution 0.7 nm) from November 16th, 2011 at 13:20 UTC at $3°59'06''$N $14°44'40''$W at a telescope elevation angle of $3°$. At 477 nm the O_4 dSCD is $(2.47 \pm 0.01) \times 10^{43}$ molec^2 cm^{-5}, the H_2O dSCD $(6.27 \pm 0.06) \times 10^{23}$ molec cm^{-2}. At 360 nm the O_4 dSCD is $(2.18 \pm 0.04) \times 10^{43}$ molec^2 cm^{-5}, the H_2O dSCD $(1.13 \pm 0.16) \times 10^{24}$ molec cm^{-2}. The fit from M91 is using one spectrum (exposure time: 60 s, spectral resolution 0.45 nm) recorded on December, 5th 2012, 19:44 UTC at $7°24'29''$S $81°30'18''$W at a telescope elevation of $3°$. It shows an O_4 dSCD of $(3.43 \pm 0.02) \times 10^{43}$ molec^2 cm^{-5} and a H_2O dSCD of $(1.18 \pm 0.16) \times 10^{24}$ molec cm^{-2}. All fits used the O_4 cross-section by Thalman and Volkamer (2013).

The retrieved water vapour dSCDs at 363 nm were compared to the 20-times stronger water vapour absorptions between 452-499 nm (20040–22124 cm^{-1}) for the *ANT XXVIII/1-2* dataset. To correct for possible influences of varying radiative

5

16

transfer conditions (which may result in different light path lengths and thus different dSCDs), the H_2O dSCDs retrieved from both spectral windows were divided by the respective O_4 dSCD from the same fitting window. These fitting intervals were selected ~~such according to~~ in a way, that the wavelength of the main absorptions of O_4 and H_2O are at ~~the same wavelength range~~ similar wavelengths. This needs to be done in order to have approximately the same radiative transfer properties for both absorbers (see subsubsection 3.3.1). The wavelength ranges are listed in Table 2. The absorption of O_4 is an indicator for the light path length, since the O_4 concentration is proportional to the square of the concentration of molecular oxygen, which has a well-defined and sufficiently constant concentration profile.

For Figure 6, measurements at an elevation angle of 3-5° with an RMS of less than 8×10^{-4} (UV) and 4×10^{-4} (VIS) were used, additionally the error of the H_2O/O_4 ratio calculated from the fit errors of both trace gases had to be below 5×10^{-21} cm^3 $molec^{-1}$ (UV) and 3×10^{-22} cm^3 $molec^{-1}$ (VIS). This implicitly removes all measurements with low O_4 dSCDs, which is the case for fog and very low clouds. These conditions lead to different numbers of valid observations in Table 3 for different spectral retrieval settings.

The scale height of O_4 is 4 km, the scale height of water vapour is typically 2 km (Wagner et al., 2013). MAX-DOAS measurements of trace gas dSCDs are most sensitive to the lowermost 2 km (e.g. Frieß et al., 2006). Thus for a given surface volume mixing ratio of water vapour, an almost constant ratio of H_2O and O_4 dSCD is expected. Figure 6 shows that this approximation is valid for the ~~ANT XXVIII~~ *ANT XXVIII/1-2* measurements, as the correlation coefficients R^2 for the individual O_4 and H_2O dSCDs are smaller (~~0.83 and 0.77~~0.81 and 0.74) than the correlation coefficient $R^2 = 0.89$ for their ratio.

However, the different profile shapes can introduce deviations, which were investigated by radiative transfer modelling using the Monte Carlo radiative transfer model McArtim (Deutschmann et al., 2011). Assuming different water vapour surface concentrations (0.1–3%), water vapour scale heights of 1,2,3 km, an aerosol layer with an extinction of 0, 0.2, 1, 2, 10 km^{-1} with a thickness of 1 and 3 km in an altitude of 0,1,2,3 km, the resulting simulated H_2O/O_4 dSCD ratios correlate for both wavelengths 363 nm and 477 nm with an $R^2 = 0.98$ and a slope of 1.00 ± 0.02. The intercept was fixed to zero. Elevation angles were $3, 5, 90°$. 6480 individual simulations were performed. A significant systematic dependence of the ratios on ground albedo, solar zenith angle and relative azimuth angle was not observed, each of them resulting in less than 1% change of the simulated O_4/H_2O ratio. Simulations with small O_4 dSCDs, which result in a large simulation error for the H_2O/O_4 dSCD ratio, were removed analogously to the measurements.

The Ångström exponent was varied using values of 0.0, 0.5 and 1.0 according to AERONET AOD measurements during *ANT XXVIII/1* (Smirnov et al., 2009)[2]. The effect on the ratio was however also smaller than 1%.

As for the measured data, the correlation of the simulated O_4 or H_2O dSCDs individually is significantly worse with $R^2_{O_4} = 0.74$ and $R^2_{H_2O} = 0.91$ compared to the correlation of their respective ratios. The slope of a linear polynomial fit to the O_4 dSCDs at 360 nm and 470 nm is similar to the observed values.

~~For , measurements at an elevation angle of 3-5° with an RMS of less than 8×10^{-4} (UV) and 4×10^{-4} (VIS) were used, additionally the error of the H_2O/O_4 ratio calculated from the fit errors of both trace gases had to be below 5×10^{-21} cm^3~~

---

[2]http://aeronet.gsfc.nasa.gov/new_web/cruises_new/Polarstern_Fall_11.html

Figure 6. Top left panel: Ratio of water vapour dSCD and O_4 dSCD at 363 nm and ~~477~~479 nm for a telescope elevation angle of 3 and 5° during *ANT XXVIII/1-2* using the O_4 cross-section by Thalman and Volkamer (2013). Error bars <u>represent typical measurement errors</u> <u>and</u> are calculated from fit errors of both absorbers. Error bars for the ratios at ~~477~~479 nm are omitted. They are more than one order of magnitude smaller than those at ~~360~~363 nm. A ratio of 10^{-20} cm^3 molec^{-1} corresponds to an absolute water vapour mixing ratio of 0.01 at ground-level or a vertical column density of $5 \cdot 10^{22}$ molec cm^{-2} or 15 kg H_2O m^{-2} assuming a scale height of 2 km. **Top right panel**: The residual of the linear fit shows a Gaussian distribution and agrees with respect to its width of $\sigma = 6.12 \times 10^{-21}$ cm^3 molec^{-1} with the mean measurement error (two times DOAS fit error, $2.75 \pm 0.92 \times 10^{-21}$ cm^3 molec^{-1}) obtained from the DOAS fit. The individual correlations of H_2O and O_4 dSCDs are shown in the **lower panels**, which show individually smaller correlation coefficients than their respective ratios at ~~360~~363 and ~~477~~479 nm.
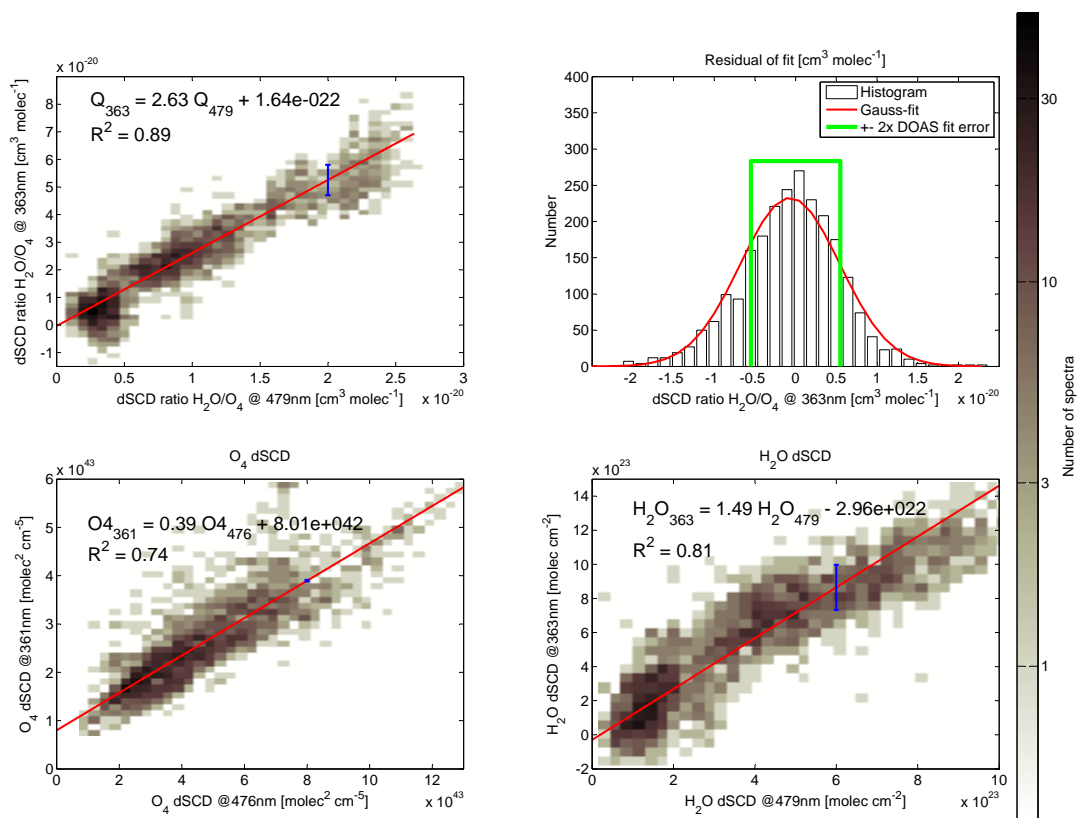
	Type	O_4 cross-section	R^2	Slope	Syst. Error [%]	Offset [cm^3 $molec^{-1}$]	n
1	MAX-DOAS	Thalman 273K	0.89	2.63(1)	8	$0.16(4) \times 10^{-21}$	2621
2	MAX-DOAS	Thalman 273K free shift	0.88	2.61(1)	8	$0.34(4) \times 10^{-21}$	2634
3	MAX-DOAS	Thalman 273K+293K	0.83	2.39(1)	8	$7.25(5) \times 10^{-21}$	2562
4	MAX-DOAS	Hermans	0.86	2.62(1)	8	$4.22(4) \times 10^{-21}$	2630
5	MAX-DOAS	Greenblatt	0.84	2.55(1)	9	$21.1(1) \times 10^{-21}$	2183
6	MAX-DOAS	Greenblatt (shifted by 0.2 nm)	0.89	2.58(1)	11	$10.1(1) \times 10^{-21}$	2586
7	LP-DOAS	Thalman 293K	0.25	2.31(25)	30	$1(3) \times 10^{-21}$	320

Table 3. Results from Figure 6 to determine the relative magnitude of the water vapour absorption at 363 nm compared to 477 nm using the HITEMP cross-section for different retrieval settings using different O_4 cross-sections. Values in brackets denote the error of the last digits of the respective value calculated from the error-weighted linear regression. For LP-DOAS measurements (see subsection 4.1) the correlation was done for SCDs instead of H_2O/O_4 dSCD ratios, because the light path was constant. The offset (LP-DOAS) was however normalized by the mean O4 dSCD at 360 nm in order to have comparable values. The systematic error of the slope was determined by using the typical relative measurement error of water vapour for measurements at a dSCD of 3×10^{23} molec cm^{-2} determined in the respective blue wavelength range.

molec^{-1} (UV) and 3×10^{-22} cm^3 molec^{-1} (VIS). This implicitly removes all measurements with low O_4 dSCDs, which is the case for fog and very low clouds.

As seen from Figure 6, the H_2O/O_4 dSCD ratios from *ANT XXVIII/1-2* correlate well for the wavelength ranges around 360 nm and around 477 nm with an $R^2 = 0.89$. However, the absolute magnitude of the absorption cross-section near ~~363nm~~ 363 nm is underestimated by a factor of 2.6 ± 0.3 (see also Table 3).

In Figure 2 the ratios of H_2O and O_4 dSCDs at 3° telescope elevation were converted to H_2O VCDs assuming a lightpath at ground level under normal conditions and a water vapour scale height of 2 km and using the correction factor of 2.6. Qualitatively the latitudinal variation of the *ANT XXVIII/1-2* and GOME-2 data agree. For a quantitative comparison further radiative transfer modelling to obtain tropospheric water vapour profiles from the ship-based data would be needed.

The O_4 cross-section is known to change its shape with changing temperature (Pfeilsticker et al., 2001; Thalman and Volkamer, 2013). As this effect could potentially introduce similar ~~latitudinal~~ dependencies as the water vapour distribution, the spectral analysis was run in addition to the original analysis including two O_4 cross-sections at 293K and 273K. This changed the slope of the correlation shown in Figure 6 by -10% from 2.63 to 2.39 (see Table 3). In addition, an increase is observed for the offset of the linear fit, which should be ideally zero. Fixing the linear regression line for high water vapour content at the observed values, this increase in the offset of the linear fit corresponds to the observed change in the slope. We therefore conclude that the observed absorption structure is not caused by the temperature dependence of the O_4 absorption cross-section, but indeed by water vapour absorption, as this offset is observed in polar regions, where almost no water vapour absorption is

expected. Note that this offset is still small and amounts to 10 % (7.25×10^{-21} cm^3 molec^{-1}) of the observed maximum ratio of H$_2$O/O$_4$ dSCDs shown in Table 3.

A spectral shift of the O$_4$ literature cross-section can effectively compensate parts of the water vapour absorption cross-section at 363 nm. This is discussed in subsection 4.5. However stable results were even obtained when the shift of the set of literature cross-sections was determined by the Levenberg-Marquardt algorithm of the DOAS fit, as shown in row (2) in Table 3.

As seen from Table 3 the resulting slopes from Figure 6 agree within their respective errors for different O$_4$ cross-sections. The O$_4$ absorption by Greenblatt et al. (1990) shows a systematic shift for the absorption at 360 nm and was therefore analysed once with the original wavelength calibration and once shifted by 0.2 nm (used e.g. in Pinardi et al. (2013)). The results of the shifted O$_4$ cross-section include more measurements but still show a significant offset of the linear regression. The results using the Hermans et al. (1999) O$_4$ cross-section seem more reliable, as more data points can be used and the offset of the slope is smaller. The most consistent results are obtained when using the O$_4$ cross-section by Thalman and Volkamer (2013), showing a small offset and the highest correlation coefficient.

4.3 Differences using different dipole moment surfaces (DMS)

The *POKAZATEL* line list employs the DMS from Lodi et al. (2011), while the *POKAZATEL (CVR)* line list employs the DMS by Lodi et al. (2008), while using the same PES. This leads to significant differences in the intensities of the resulting line lists in the near-UV spectral region. The magnitude of the absorption between 362–365 nm in *POKAZATEL (CVR)* is on average 2.9 (ranges between 2.3–4.6) times larger than in *POKAZATEL*, and might therefore explain the observed discrepancy in the magnitude of the cross-section shown in subsection 4.2. However, the shape of the absorption band in the atmospheric measurements is significantly better predicted by *POKAZATEL*. Fitting *POKAZATEL (CVR)* to measured spectra from M91 leads to 20% higher RMS of the residual (see Figure 7) at low elevation angles. The additional absorption structures around 354 nm listed in *POKAZATEL (CVR)* are not found in observations (compare also Figure 10). These findings are consistent with the spectral analysis of data from *ANT XXVIII/1-2* .

POKAZATEL (CVR) also predicts water vapour absorption between 330-360 nm, which should be above our detection limit. These could however not be identified for either of the two line lists during the M91 cruise (see also subsection 4.6).

4.4 Comparison to other line lists

As shown in Figure 1, other water vapour line lists also contain lines in the spectral range below 390 nm, which should be theoretically above typical detection limits of our measurements (often better than 10^{-4} along a light path of 10km). However in this spectral range BT2 and HITEMP are based on calculations only and have not yet been confirmed by laboratory or atmospheric measurements. The absorption at 380 nm should be clearly above the detection limit of the instrument used during M91, but as reported in Lampel et al. (2015b), it was not unambiguously found and showed inconsistencies. These two line lists show further absorption lines between 330–360 nm, which could also not be identified in Lampel et al. (2015b).
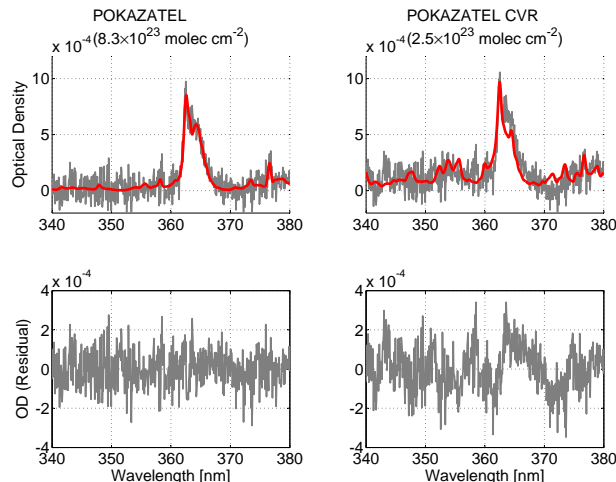
Figure 7. Two MAX-DOAS fits of the same measurement spectrum from M91 showing the detection of water vapour absorptions at 363 nm using two different DMS (see subsection 4.3). In order to reduce residual noise, the fit is using four spectra with a total exposure time of 240 s recorded on December, 22nd 2012, starting at 17:59 UTC at $15°31'$S $75°36'$W at a telescope elevation of $3°$. The *POKAZATEL (CVR)* line list shows a 20% larger residual than *POKAZATEL*, whose shape fits the observed optical density better.

Fitting simultaneously a cross-section based on *POKAZATEL* and a cross-section based on HITEMP or BT2 to the measurements (M91), the optical density (from 340–380 nm) attributed to BT2 and HITEMP remained below $(3\pm12)\%$ and $(2\pm8)\%$, respectively, of the optical density of the water vapour absorption attributed to the *POKAZATEL* cross-section. The optical density attributed to BT2 and HITEMP was $(-1\pm6)\times10^{-5}$ and $(-1\pm4)\times10^{-5}$, respectively, while the *POKAZATEL* cross-section showed absorptions of $(4.5\pm4.3)\times10^{-4}$ for all spectra at all elevation angles of the M91 dataset with ~~a~~ an RMS of the residual of less than 4×10^{-4}.

These findings demonstrate that the shape of the water vapour absorption appears to be better predicted in the *POKAZATEL* line list than in ~~either~~ the BT2 and the HITEMP line list. For HITEMP this was expected, since HITEMP is partly based on BT2, but ~~a large number of individual lines had been removed due to~~ the individual line intensity ~~cut-off of 10^{-27} cm molec^{-1} for these wavelengths (Rothman et al., 2010). This procedure~~ cutoff leads to changes in absorption band shape and the significantly smaller water vapour absorption cross-section in HITEMP compared to BT2 as shown in Figure 1.

4.5 Compensation of H$_2$O absorption by O$_4$ absorption near 363 nm

Since the water vapour absorption is found at the red flank of the O$_4$ absorption band at 361 nm, the absorption can be partly compensated by shifting the O$_4$ absorption band towards longer wavelengths. This effect is more clearly observed for the ~~ANT XXVIII~~ *ANT XXVIII/1-2* data-set than for the M91 data-set, due to the lower spectral resolution, which seems to match better the widths of the spectral absorption structures of O$_4$.
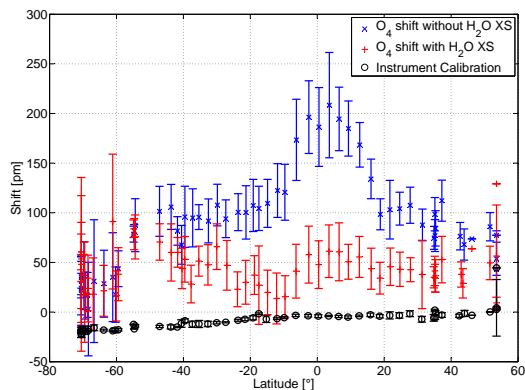
Figure 8. Error weighted daily averaged DOAS fit results for the shift of the O_4 cross-section for measurements with a signal-to-noise ratio for the O_4 dSCD of more than 50. For this evaluation, the shift of the O_4 cross-section was freely determined by the DOAS fit and not linked to the other absorption cross-sections. Error bars denote the standard deviation during one day. The shift of the instrumental calibration was determined from fit of the measured spectra to data from a convolved solar atlas.

When evaluating the *ANT XXVIII/1-2* data-set using the same settings as listed above in Table 2, but allowing for a spectral shift of the O_4 cross-section by Thalman and Volkamer (2013), a systematic shift of the O_4 cross-section of up to 0.20 nm relative to a Fraunhofer reference calibrated using the solar atlas of Chance and Kurucz (2010) is observed in tropical regions (shown in Figure 8). A systematic shift of the O_4 cross-section of up to 0.15 nm relative to a freely shifting O_4 cross-section

5 from a fit including the *POKAZATEL* water vapour absorption cross-section is observed. When the water vapour absorption is included, the free shift of the O_4 cross-section shows a standard deviation of 0.035 nm for measurements with a signal-to-noise ratio of more than 50 for the O_4 dSCD. The instrument calibration shows a standard deviation of 0.007 nm due to a slow drift of 0.3 pm d^{-1}.

It was found that a small shift of O_4 with temperature (e.g. 0.05 nm as in Thalman and Volkamer (2013) from 273K–293K)

10 cannot explain the apparent shift of the O_4 absorption when not considering the water vapour absorption.

As described in Beirle et al. (2013), a spectral shift can be linearised for small shifts by the derivative of the absorption cross-section with respect to wavelength using Taylor expansion. Turning the argument around, therefore a correlation of the size of the absorption structure of water vapour and the product of O_4 absorption and spectral shift (from a DOAS fit where water vapour absorptions are not considered) is expected. This correlation is found for *ANT XXVIII/1-2* data with $R^2 = 0.89$ and

15 a slope of $a_S = 6.78 \times 10^{18}$ nm molec cm^{-3}. For this instrument with a spectral resolution of 0.7 nm it thus means effectively that a water vapour dSCD of $S_{H_2O} = 5 \times 10^{23}$ molec cm^{-2} and an O_4 dSCD of $S_{O_4} = 2.5 \times 10^{43}$ molec^2 cm^{-5} leads to a shift of the O_4 cross-section by $a_S \cdot S_{H_2O}/S_{O_4} = 0.14 nm$, which was indeed observed in tropical regions as shown in Figure 8. The change in overall O_4 dSCD is discussed in subsection 4.11.

22

4.6 Upper limit for water vapour absorption at 335 nm

The water vapour absorption band at 335 nm in the *POKAZATEL* line list would amount to an OD of 1.2×10^{-4} for a water vapour dSCD of 4×10^{23} molec cm^{-2} at a spectral resolution of 0.5 nm.

Analogous to the procedure described in subsection 4.2, the water vapour absorption band at 335 nm (fit range 332–358 nm) was compared to the water vapour absorption within the interval from 452-499 nm for the *ANT XXVIII/1-2* measurements, divided by the dSCD of the respective O$_4$ absorption band. A clear correlation was not observed ($R^2 < 0.2$) due to too large fit errors to detect water vapour in the BrO/HCHO fit range (fit settings: Table 2). The water vapour dSCD (at 335 nm) stayed below the average detection limit of 7×10^{23} molec cm^{-2} .

For the M91 MAX-DOAS measurements the detection limit was reduced by co-adding 16 elevation sequences. However, the correlation of water vapour dSCDs at 335 nm and 442 nm was small ($R^2 = 0.2$) and the 2σ detection limit of 6.5×10^{23} molec cm^{-2} was only exceeded for 10% of all spectra.

We therefore conclude that the predicted magnitude of the absorption at 335 nm is correct or overestimated, as we could not find it in our MAX-DOAS observations: If the shape of the water vapour absorption is correctly predicted by *POKAZATEL*, the magnitude of the differential water vapour cross-section from 332–358 nm at a spectral resolution of 0.45 nm-0.70 nm is smaller than 2.5×10^{-28} cm^2 molec $^{-1}$.

4.7 Water vapour absorption around 376 nm

The literature values for the water vapour absorption cross-sections based on *POKAZATEL* and BT2 (and thus also HITEMP) differ by about one order of magnitude in the spectral region between 370 and 380 nm (compare Figure 1). Using the M91 MAX-DOAS measurements the absorptions listed in BT2 could not be unambiguously identified or its predicted absorption shape did not match the observed absorptions. We therefore apply here the *POKAZATEL* line list on data from the M91 campaign.

We use a fit range from 370-386 nm and the settings for the water vapour absorption at 363 nm without considering the ~~water~~ absorption cross-section of O$_3$, HONO, BrO and HCHO. Co-added spectra based on four elevation sequences were used in order to reduce the average fit error to 2×10^{23} molec cm^{-2} (average RMS of the residual: 1.1×10^{-4}). The water vapour dSCD was compared to the water vapour dSCD from 340-380 nm, retrieved in section 4.2. The resulting correlation of dSCDs at 363 nm and 376 nm is significant with R^2=0.6 and a slope of 1.2 ± 0.3. A DOAS fit result is shown in Figure 9. As both absorption bands are at similar wavelengths and the absorptions are small, the difference in expected dSCDs introduced by differences in radiative transfer are negligible compared to the measurement error itself.

This shows that the water vapour absorptions at 376 nm is found in MAX-DOAS measurements and its magnitude is predicted in agreement with the absorption at 363 nm. It underestimates the absorption inferred from measurements by a factor of 3.1 ± 0.7.
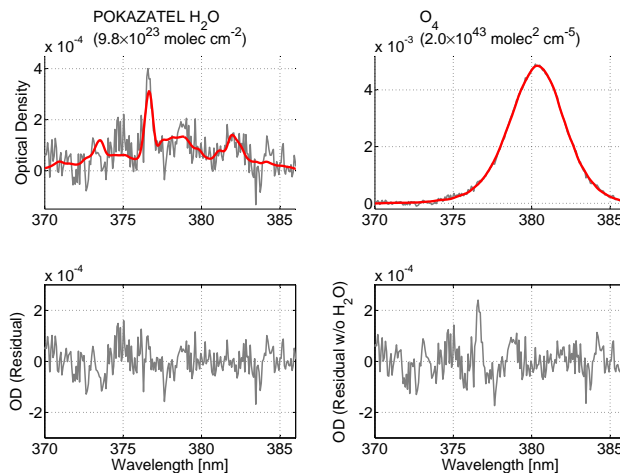
Figure 9. Fit result for the same MAX-DOAS spectrum as used in Figure 7 to show the water vapour absorption at 376 nm, which correlates for the M91 dataset with R^2=0.6 and a slope of 1.2 ± 0.3 with the water vapour absorption at 363 nm. The measurement error of this individual fit amounts to 20%.

4.8 Water vapour absorption below 330 nm

Du et al. (2013) reported significant water vapour absorptions of up to 2.94×10^{-24} cm^2 molec^{-1} at 330 nm and up to 2.19×10^{-24} cm^2 molec^{-1} at around 315 nm. Lampel et al. (2015b) could not confirm these findings and found upper limits for the differential absorption of water vapour from 332–370 nm of 3×10^{-27} cm^2 molec^{-1} from the M91 dataset which are two

5 orders of magnitude smaller. Wilson et al. (2016) also could not confirm the values published by Du et al. (2013) between 325–420 nm. They estimated the water vapour absorption cross-section at a spectral resolution of 0.5 nm to be less than 2×10^{-25} cm^2 molec^{-1}.

For a water vapour dSCD of 4×10^{23} molec cm^{-2} , the findings of Du et al. (2013) would result in differential optical depths around unity, which is unrealistic judging from observations of BrO and HCHO in the troposphere in wavelength

10 intervals within 330–360 nm (see references listed in Vogel et al. (2013) and Pinardi et al. (2013)). The instrument operated during *ANT XXVIII/1-2* covers a wider spectral range than in Lampel et al. (2015b), we therefore applied the BrO/HCHO fit settings from Table 2 to a fit interval from 310–350 nm. ~~The~~ We used the water vapour dSCD ~~was obtained from the absorption listed in~~ determined from *POKAZATEL* at ~~364~~363 nm ~~divided by 2.63 as shown in to estimate the expected dSCD in this fit interval. A polynomial of~~ of 4.3×10^{23} molec cm^{-2} for the spectrum from *ANT XXVIII/1-2* shown in Figure 5. For the

15 calculation of the upper limit we used conservatively only half of the value of the dSCD in order to account for the shorter light path at wavelengths between 310–350 nm. Polynomials with degree 0–2 ~~was~~ were applied in the fit in order to account broad-band absorptions and scattering ~~. The~~ and to estimate the dependence of the inferred upper limits on the degree of the DOAS polynomial. The polynomial could compensate for water vapour absorption if it would be a rather broad absorption in this spectral region as suggested by Du et al. (2013). The resulting peak-to-peak (ptp) magnitudes of the residual are listed

24

Polynomial degree	ptp residual	upper limit diff. H_2O XS cm^2 molec^{-1}
0	3.0×10^{-3}	14.0×10^{-27}
1	1.6×10^{-3}	5.4×10^{-27}
2	1.0×10^{-3}	4.6×10^{-27}

Table 4. Magnitude peak-to-peak (ptp) residual sizes and upper limits for water vapour absorption between 310 and 350nm at a spectral resolution of 0.7 nm for different polynomial degrees of the DOAS polynomial~~using the water vapour dSCD determined from at 363 nm of for the spectrum from shown in .For the calculation of the upper limit we used conservatively only half of the value of the dSCD in order to account for the shorter light path at wavelengths between 310–350 nm.~~

for an example measurement spectrum at 3° <u>elevation angle</u> in Table 4. To avoid unnecessary compensation of potential water vapour absorption by other absorbers, their dSCDs were determined using a DOAS polynomial of third order, then the dSCDs of the trace gases in the fit were fixed to these values.

The resulting upper limits for the water vapour absorption cross-section in the spectral range from 310–350 nm are thus 200–600 times smaller than the maximum cross-section values measured by Du et al. (2013) and are 14–33 times smaller than the upper limit value presented in Wilson et al. (2016).

4.9 Estimation of the accuracy of the <u>shape and wavelength calibration of the POKAZATEL</u> H_2O cross-section

The DOAS fit provides dSCDs as mentioned above, but also residual spectra**R_i.**. These residual spectra are the difference between the modeled and the observed OD (compare Figure 5). In order to disentangle different contributions to the residual spectra, a multi-linear regression was performed based on the retrieved dSCDs (see Lampel et al., 2015a). This allows the systematic identification of residual structures caused by each of the absorbers considered in the fit (compare Table 2). However, since potential differences between modeled and observed absorptions can be compensated by any of the other absorbers, this information cannot be used to correct a given absorption cross-section. It can yield an estimate of the accuracy of the cross-section.

For *ANT XXVIII/1-2* , the resulting spectrum from 340–380 nm which correlates with the water vapour dSCD (shown in Figure 10) has an RMS of 1.7×10^{-28} cm^2 molec^{-1} and a maximum peak-to-peak amplitude of 1.1×10^{-27} cm^2 molec^{-1}. The maximum magnitude of water vapour absorption cross-section at 363 nm is 2.5×10^{-27} cm^2 molec^{-1} for this spectral resolution (see Figure 1). For M91, a residual structure at 344 nm is found, which could not be attributed to other absorbers and is correlated with the water vapour dSCD. <u>The variation of humidity during M91 is significantly less than during</u> *ANT XXVIII/1-2* <u>, therefore this structure could have been caused by any tropospheric absorber with a similar concentration height profile.</u> As this residual structure is not observed for both datasets, we do not attribute it to water vapour absorption.
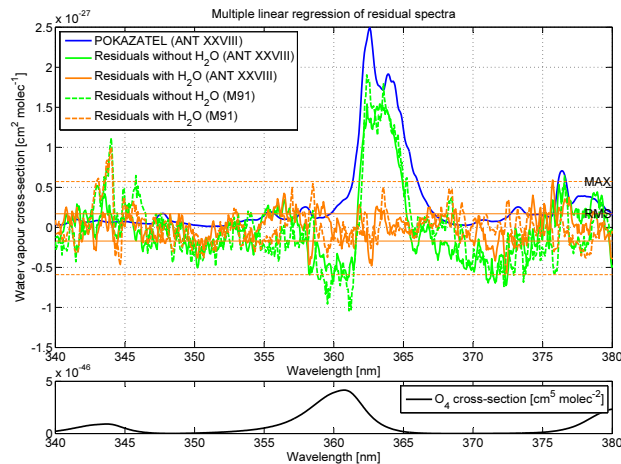
Figure 10. Using a multi-linear regression on the residual spectra from the campaigns *ANT XXVIII/1-2* and M91, the water vapour dSCD-correlated residual structures were obtained. Negative values can be explained by compensation of the missing water vapour absorption structures by other absorbers included in the DOAS fit. The resulting spectrum including water vapour absorption yields an estimate on the accuracy of the convolved cross-section.

The maximum absorption of water vapour at 363 nm according to *POKAZATEL* seems to be red-shifted by 0.5 nm relative to the maximum absorption listed in BT2 (see inset in Figure 1). To test if the wavelength of the water vapour absorption is correct, a spectral shift of the water vapour absorption was allowed, i.e. the shift was determined by the Levenberg-Marquardt algorithm of the DOAS fit. As the spectral resolution is higher, this was done for the M91 measurements. The shift of the

5   *POKAZATEL* water vapour absorption was found to agree with observations within 0.02 ± 0.06 nm (corresponding to $1.5 \pm 4.6 \, \mathrm{cm}^{-1}$) for measurements exceeding a signal to noise ratio for the water vapour dSCD of 5 for the 16 elevation sequence co-added M91 dataset. This result is in agreement with the estimate of the precision of the PES by Polyansky et al. (2016), which was able to reproduce energy levels from laboratory measurements within about $0.1 \, \mathrm{cm}^{-1}$ on average.

4.10   Further potential error sources

10   As the observed OD for water vapour absorption were small in the UV ($< 2\%$ for individual absorption lines at high spectral resolution), no saturation correction (Wenig et al., 2005) was applied during convolution of the line list for the spectral retrieval of MAX-DOAS data. The *POKAZATEL* line list does not provide line broadening parameters, therefore also the I_0 correction (Platt et al., 1997) was not applied. This correction would have resulted in a change of the convolved cross-section of less than 5%.

15   In the visible (452-499 nm), the saturation effect for dSCD of $6 \times 10^{23} \, \mathrm{molec \, cm}^{-2}$ amounts to less than 2% change of the obtained dSCD.

26

4.10.1 Uncertainties of the H_2O literature cross-sections in the blue wavelength range

Since we compared the UV absorptions of H_2O vapour to the values derived in the blue spectral region the errors in the latter spectral region - which we analyse in the following - enter into the calculation of the total uncertainty of the UV absorption cross sections of H_2O.

5   The uncertainty of the absolute magnitude of water vapour cross-section (HITEMP) in the blue wavelength from 452-499 nm ~~introduces an uncertainty of~~ is less than 15%: The 6ν absorption band around 490 nm seems to be overestimated by $(13 \pm 3)\%$ relative to the $6\nu + \delta$ absorption band around 470 nm when fitting the absorption bands separately analogously to Lampel et al. (2015b). This is one of the main reasons for the strongly structured fit residual in the visible fit range shown in Figure 5.

10   The magnitude of the $6\nu + \delta$ absorption band around 470 nm agreed with the magnitude of the 7ν absorption band around 440 nm according to LP-DOAS measurements by Lampel et al. (2015b), for which in turn an agreement within 10% with independent measurements of humidity and temperature was found in the same publication.

4.10.2 Uncertainties of the O_4 literature cross-sections

For constant atmospheric water vapour content, water vapour and O_4 dSCDs from MAX-DOAS observations are typically well-
15 correlated because the bulk of the variations in the ~~H2O-dSCD~~ H_2O-dSCD is due to variations in the path-length. Therefore it is important to disentangle potential problems of the water vapour absorption cross-section and O_4 absorption cross-section. The three available O_4 cross-sections for the spectral range below 400 nm were published by Greenblatt et al. (1990), Hermans et al. (1999) and Thalman and Volkamer (2013). The *POKAZATEL* water vapour line list shows a local maximum at 363 nm (at a spectral resolution of 0.45 nm) which is at the slope of the O_4 absorption peak at 360.8 nm (see Figure 1).

20   Differences in differential OD from 340 nm to 390 nm between different literature O_4 cross-sections amount to up to 2×10^{-3} for a typical dSCD of O_4 of 4×10^{43} molec^2 cm^{-5}. This is larger than the OD of water vapour in this spectral range as listed in *POKAZATEL*. A systematic error in the respective O_4 cross-section which could lead to false apparent water vapour absorption, ~~which~~ is expected to scale with the column density of O_4 ~~and~~. It would thus result in a constant offset of the correlation of H_2O / O_4 ratios shown in Figure 6. This was not observed. This also agrees with the observation that the
25 wavelength dependence of the O_4 dSCDs was found to have no result on the water vapour dSCD at 363 nm. Thalman and Volkamer (2013) state an absolute accuracy of 2–4% for the their integrated O_4 absorption cross-section at 361 nm and 476 nm.

    For strong absorbers, the AMF of the observation also depends on the magnitude of the absorption itself (Marquard et al., 2000; Pukīte et al., 2010). However, for an optical density of O_4 at 360.8 nm of 2.5×10^{-3} we estimate a reduction of the effective light path by less than 1.3%~~, which~~. This is an OD of less than 3.5×10^{-4} and would result in a reduction of
30 the apparent water vapour dSCD by 10%. This effect would be smaller by a factor of 4 in tropical regions due to a smaller contribution of the O_4 absorption to the total optical depth. No ~~direct~~ correlation of the water vapour dSCDs at 363 nm with the ~~O_4 dSCDs~~ square term of the O_4 absorption was found for the *ANT XXVIII/1-2* dataset.

Trace gas	Wavelength nm	RMS	rel. Change of dSCD per H_2O dSCD	Typ. diff.
O_4	340–380	-25%	$+2.9 \times 10^{18}$ molec cm^{-3}	+5%
HONO	337–375	-18%	$+1.4 \times 10^{-9}$	+22 ppt
OClO	332–370	-20%	$+3.1 \times 10^{-11}$	+0.5 ppt
SO_2	337–375	-20%	-2.3×10^{-7}	-3.6 ppb

Table 5. Impact on spectral retrievals estimated from DOAS evaluations with and without accounting for the water vapour absorption from *POKAZATEL* for the M91 MAX-DOAS data set (at a spectral resolution of 0.45 nm or 34 cm^{-1} at ~~362.3~~363 nm/~~27601~~27548 cm^{-1}). The typical difference was estimated for a water vapour dSCD of 4×10^{23} molec cm^{-2} along a 10 km long light path.

The differences between the cross-sections published by Thalman and Volkamer (2013), Greenblatt et al. (1990) and Hermans et al. (1999) did not allow to identify any systematic differences similar to the water vapour absorption, which could have pointed towards water vapour ~~absorption~~ contamination during the acquisition of the cross-section data.

As seen in Table 3, it was possible to observe good correlations for water vapour absorption at 363 nm and around 477 nm for all available O_4 literature cross-sections. The smallest offset is observed when using the O_4 cross-section by Thalman and Volkamer (2013). The best correlation coefficients R^2 are found for Thalman and Volkamer (2013) and Hermans et al. (1999).

Absolute maximum O_4 absorption cross-section values differ for the three available cross-sections at 293K by less than 7% at 360 nm and less than 5% at 477 nm. This uncertainty could directly affect to the H_2O/O_4 ratios listed in Table 3.

4.11 Influence on DOAS retrievals of other trace gases

Neglecting the water vapour absorption around 363 nm increases not only the fit errors of several DOAS trace-gas retrievals, but could also introduce a systematic bias in the trace gas concentrations obtained. Trace gas species which are potentially influenced are O_4, HONO, OClO and SO_2.

The effect may vary for different data-sets, different DOAS-fit intervals and different instrumental parameters such as the respective spectral resolution. Here the impact on trace-gas retrieval is investigated based on M91 MAX-DOAS data set using the settings listed in Table 2. Only fit results with an initial RMS of the fit residual of less than 4×10^{-4} were considered.

4.11.1 O_4 (340–380 nm)

For MAX-DOAS observations, the effective light path length needs to be determined to convert observed slant column densities into concentrations of the respective trace gas. The absorption of the oxygen dimer O_4 can be used to infer information about atmospheric light paths (e.g. Wagner et al., 2002). Atmospheric aerosol extinction profiles can be estimated by constraining the input parameters of radiative transfer models to match the observed O_4 column densities. For MAX-DOAS measurements this approach has been described e.g. in Wagner et al. (2004); Frieß et al. (2006). However, for some observations of scattered

sunlight, the absorption of O_4 had to be corrected by a correction factor in order to explain the measured column densities as reported by (e.g. Wagner et al., 2009; Clémer et al., 2010; Irie et al., 2015). Clémer et al. (2010) estimated a correction factor value of $1.2-1.5$ for modelled differential slant column densities (dSCD) values to match observed dSCDs. The reason for this correction factor is so far unknown. However, for direct-sun DOAS measurements and measurements in the tropopause (Spinei et al., 2015) showed that a correction factor is not necessary to explain the measurements. Recently a possible explanation for a part of these previous observations was provided by Ortega et al. (2016): elevated aerosol layers in heights above 2 km which affected the apparent O_4 dSCDs but could not be resolved from ground-based MAX-DOAS measurements due to their limited information content for aerosol extinction in these altitudes. Another reason for this correction factor could be an unaccounted tropospheric absorber, such as e.g. water vapour absorption.

To estimate the effect of water vapour absorption, the same evaluation for O_4 according to Table 2 was performed once with and once without the *POKAZATEL* water vapour absorption cross-section. An increase in O_4 dSCD is observed when including the *POKAZATEL* water vapour absorption cross-section in the DOAS evaluation.

Using the correction factor of 2.63 determined in Figure 4.2, including the water vapour absorptions leads to an increase in O_4 dSCD per H_2O dSCD of $+(2.9 \pm 0.3) \times 10^{18}$ molec cm^{-3}, independent of the settings whether a shift and/or squeeze is allowed for the literature absorption cross-sections.

For a typical H_2O dSCD of 4×10^{23} molec cm^{-2} in summer at mid-latitudes and a O_4 dSCD of 2.5×10^{43} molec^2 cm^{-5} (10 km light path length) including the water vapour absorption leads to an absolute increase of O_4 dSCD of 1.2×10^{42} molec^2 cm^{-5} , which corresponds to a change of $+5.0\%$.

Thus the water vapour absorption at 363 nm cannot explain the correction factor for O_4 dSCDs introduced in various publications(see), it even increases the factor by $+5.0\%$ for measurements during summer in mid-latitudes.

4.11.2   HONO (337–375 nm)

Nitrous acid (HONO) is a key species in the atmospheric chemistry of urban air-masses (e.g. Perner and Platt, 1979), because its photolysis leads to the production of OH radicals, the 'detergent' of the atmosphere. Due to its high reactivity and fast daytime photolysis, HONO concentrations are low, in particular during daylight hours (Wong et al., 2012)(Wong et al., 2012; Wang et al., 2016), and thus their measurements are difficult, but can be performed e.g. by absorption spectroscopy. If all relevant absorbers are accounted for, spectroscopic measurements have the advantage of being less affected by interferences, which were observed for wet chemical methods, such as e.g. LOPAP (e.g. Kleffmann and Wiesen, 2008). Therefore it is important to account for all possible absorbing trace gas species in the respective wavelength range, e.g. 337–375 nm (Hendrick et al., 2014), in order to further reduce the detection limit and eliminate potential biases.

Adapting the wavelength range from (Hendrick et al., 2014, and using the settings listed in Table 2)(Hendrick et al., 2014) and using the settings listed in Table 2, neglecting the water vapour absorption in the HONO fit has led to an decrease of HONO dSCDs. The decrease is clearly correlated to the water vapour dSCD and amounts per corrected H_2O dSCD to 1.4×10^{-9}. This corresponds for a H_2O dSCD of 4×10^{23} molec cm^{-2} to a negative bias of HONO dSCDs by 5.6×10^{14} molec cm^{-2} , which corresponds to a HONO surface volume mixing ratio of 22 ppt along a light path of 10 km.

The RMS decreases for this water vapour dSCD by 0.4×10^{-4} at a typical RMS of 2.2×10^{-4}, which is a decrease of 18%.

This decrease of dSCDs explains negative HONO dSCDs around noon during M91, when not considering water vapour absorption.

At an elevation angle of $3°$ we obtain a distribution of dSCDs around $(-3.9 \pm 2.4) \times 10^{14}$ molec cm^{-2} without including water vapour absorption. Including the water vapour absorption, the HONO dSCDs are distributed around $(1.0 \pm 2.3) \times 10^{14}$ molec cm^{-2}. During the cruise significant positive HONO dSCDs were observed close to NO$_2$ plumes from cities (HONO dSCDs of up to 2×10^{15} molec cm^{-2} at low telescope elevation angles), when the cruise track was close to the Peruvian coast. Therefore a slightly positive average HONO dSCDs can be expected., but it is in agreement with zero within the standard deviation of the observed values. Filtering the results based on HONO dSCDs could have introduced a negative bias, as the observed HONO values are generally close to the respective detection limits. We therefore used the complete MAX-DOAS data set.

4.11.3 OClO (332–370 nm)

Stratospheric OClO has been observed in polar regions (e.g. Solomon et al., 1987; Kühl et al., 2008; Oetjen et al., 2011). Recently, OClO has also been observed in volcanic plumes (Bobrowski et al., 2007; Theys et al., 2014; Donovan et al., 2014; General et al., 2015; Gliß et al., 2015). All of these measurements were limited on one side of the retrieval interval close to 360 nm, potentially indicating unaccounted absorptions or erroneous O$_4$ cross-sections. Saiz-Lopez and von Glasow (2012) and references therein suggested that so far tropospheric OClO outside volcanic plumes has been observed only in polar regions with small absolute tropospheric water vapour content.

The 363 nm water vapour absorption band is located between two absorption bands of OClO and thus neglecting the water vapour absorption leads to an underestimation of OClO dSCDs and systematic residual structures.

Even when including water vapour absorption according to *POKAZATEL*, OClO was not positively identified during M91 (332–370 nm) above a 2σ detection limit of 1.6×10^{13} molec cm^{-2} at an elevation angle of $3°$, the dSCDs showed a distribution around $(-0.9 \pm 8.0) \times 10^{12}$ molec cm^{-2}. Without correction for water vapour absorption the dSCDs showed a distribution around $(-6.3 \pm 8.9) \times 10^{12}$ molec cm^{-2}.

Corrected by the scaling factor of 2.63 from Figure 4.2, the increase in OClO dSCD per H$_2$O dSCD amounts to 3.08×10^{-11}. The difference in OClO is clearly correlated with the H$_2$O dSCD with $R^2 = 0.9$. This corresponds for a H$_2$O dSCD of 4×10^{23} molec cm^{-2} to an increase of OClO dSCD by 1.2×10^{13} molec cm^{-2}, which corresponds to a OClO surface volume mixing ratio of 0.5 ppt along a light path of 10 km.

4.11.4 Impact on the retrieval of other absorbers

In the spectral region below 360 nm, concentrations of HCHO and BrO can be retrieved. For HCHO systematic problems were discussed in Pinardi et al. (2013) and pointed towards uncertainties of the available O$_4$ cross-sections. The absorptions listed within this fit range (336.5-359 nm) in BT2 are of similar magnitude as BrO concentrations for the lower troposphere as reported by (Richter et al., 2002; Volkamer et al., 2015). *POKAZATEL* also lists lines here. So far, the absorption at 335 nm could

not be unambiguously identified in measurements but can potentially have an impact on the spectral retrievals of tropospheric BrO and HCHO (see subsection 4.6).

For very high column densities of SO_2, ~~alternative~~ DOAS evaluation wavelength intervals above 340 nm can be used in order to minimize saturation effects due to large optical depths (Bobrowski et al., 2010; Hörmann et al., 2013). If such spectral evaluation schemes are applied to ground-based MAX-DOAS measurements using also low telescope elevation angles for locations with high absolute water vapour concentrations, water vapour absorption might need to be considered also in the spectral evaluation of SO_2. We estimated the impact using the HONO (337–375 nm) fit settings with the additional SO_2 absorption cross-section from Vandaele et al. (2009) in Table 5. The overall change in dSCD was of the same magnitude as the fit error ~~itself~~ (see Table 5).

4.12 MAX-DOAS: Relative water vapour absorption band strengths in the blue spectral range

The consistency of the *POKAZATEL* line list with other line lists and measured absorption was checked in analogy to Lampel et al. (2015b) in the blue spectral range for MAX-DOAS observations. The relative absorption strength relative to the much stronger absorption band around 442 nm, which is called W3 here, was determined for the *POKAZATEL* water vapour line list. The different wavelength intervals are listed in Table 6. The same MAX-DOAS data set (M91) and the same settings as described in Lampel et al. (2015b) were applied. The magnitude of the absorptions W0 and W1 are underestimated compared to MAX-DOAS observations, leading to the observation of water vapour dSCDs, which are 26%(W0) and 71%(W1) larger than the dSCDs observed simultaneously for the stronger absorption W3. The results are shown in Table 7 and Table 8.

Overall, *POKAZATEL* predicts the integrated absorption cross-sections in the blue spectral range until 480 nm range better than previous versions of HITRAN and BT2, as seen from Table 6 and summarized in Figure 11. It was however not used as a reference cross-section in the blue wavelength range, as HITEMP (and HITRAN2012) reproduced the observed water vapour absorptions in the blue fit interval (452–499 nm) significantly better. These differences which are also seen from Figure 1 will require further investigation, as they do not only involve a difference of the overall absorption strength of both bands near 470 and 490 nm, but also differences in the shape of the absorption bands were observed between HITEMP and *POKAZATEL* (see also subsubsection 4.10.1).

5 Conclusions

The water vapour absorption structure predicted from calculations for wavelengths around 363 nm by Polyansky et al. (2016) was found for the first time in two different MAX-DOAS measurement data-sets of tropospheric air-masses with optical depths of up to 2×10^{-3} at a spectral resolution of 0.45–0.7 nm. Additionally it was observed for the first time in LP-DOAS observations. Until now, to our knowledge these absorptions were neither experimentally verified nor considered in the spectral analysis of DOAS observations.

Comparing the ~~strenghts~~ strengths of the UV absorption lines of water vapour to the water vapour absorptions listed in HITEMP between 452 and 499 nm showed that the absorptions are indeed caused by water vapour and that the cross-section
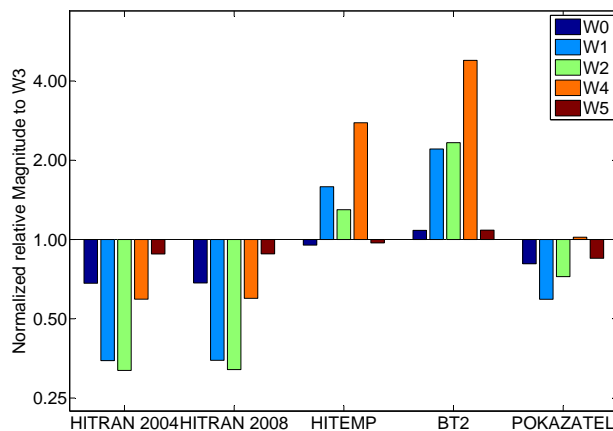
Figure 11. Comparison of different available water vapour cross-section data in the blue spectral range using ~~the~~ different ~~band~~ bands listed inTable 6. W3 was used as a respective reference in all cases and is therefore by definition unity. All magnitudes were normalized with respect to the rescaled HITEMP absorption cross-section from Lampel et al. (2015b) to obtain relative magnitudes of each of the absorption bands W0,W1,W2,W4 and W5. A value of ~~'1'~~ unity identifies good agreement with the relative magnitude of the absorption bands' sizes according to MAX-DOAS and LP-DOAS measurements presented in Lampel et al. (2015b).

calculated from the data provided by Polyansky et al. (2016) underestimates the measured absorption by a factor of 2.6 ± 0.5. For MAX-DOAS, the different light path lengths in the two different wavelength windows were corrected by normalization with the respective O_4 dSCD in the same wavelength interval. The water vapour absorption feature at 363 nm in MAX-DOAS measurements was identified and shown to be independent of the chosen literature value of the O_4 absorption cross section, i.e.

5   it was found to be at a similar magnitude for all three available O_4 literature absorption cross-sections. It was also independent of the temperature-induced broadening of the O_4 cross-section.

In contrast, a slight spectral shift of the O_4 reference spectrum could have compensated in previous evaluations (not including the 363 nm H_2O absorption) for the water vapour absorption, which is located on a slope of the O_4 absorption (subsection 4.5). This apparent shift might have lead to wavelength calibration corrections of O_4 literature cross-sections in previous publications

10   for individual campaigns with relatively constant H_2O/O_4 dSCD ratios.

Other predicted water vapour absorption features at 335 nm could not be unambiguously identified in the measurements as ~~they~~ these did not exceed the respective detection limits. The absorption structure at 377 nm was slightly above the detection limit and was found to correlate with the water vapour absorption at 363 nm.

The identified water vapour absorption at 363 nm can have a significant impact on the retrieval of trace-gases, which absorb

15   in the same wavelength range, namely O_4, HONO, OClO and SO_2. For measurement locations with high absolute water vapour concentrations, consideration of the water vapor absorption at 363 nm, if included in the spectral analysis of MAX-DOAS measurements, will lead to a reduction of measurement errors and will thus lower the overall limit of detection. We showed that neglecting this absorption introduce systematic biases in their spectral analysis:

Dominating Polyad		8ν	$7\nu+\delta$		7ν		$6\nu+\delta$
Name		W0	W1	W2	**W3**	W4	W5
Start of interval	[nm]	394.0	410.0	423.5	**434.0**	451.5	461.5
End of interval	[nm]	410.0	423.5	434.0	**451.5**	461.5	480.0
Source of cross-section data	$[10^{-27}\ \mathrm{nm\ cm^2}]$			integrated cross-section			
HITRAN 2000		0.00	0.00	0.00	**69.02**	0.00	31.03
HITRAN 2004		13.62	3.11	0.89	**96.75**	0.87	42.25
HITRAN ~~2009~~ 2008 v2009	Rothman et al. (2009)	13.71	3.13	0.90	**97.07**	0.88	42.46
HITEMP	Rothman et al. (2010)	21.01	15.73	4.01	**106.90**	4.50	51.44
BT2	Barber et al. (2006)	26.05	23.84	7.86	**116.50**	8.46	62.67
HITEMP rescaled	Lampel et al. (2015b)	22.06	9.91	3.09	**106.90**	1.62	52.98
POKAZATEL	Polyansky et al. (2016)	15.98	5.26	2.00	**95.7**	1.48	40.26

Table 6. Integrated absorption in $[10^{-27}\ \mathrm{nm\ cm^2}]$ over each of the wavelength intervals W0-W5 for different sources of cross-section data. Not only for the largest absorption structure W3 variations between the different compilations are seen, but especially ~~relative~~ integrated absorption values relative to W3 vary. The ~~last row shows the maximum optical density for a water vapour column density (CD) within each wavelength interval at a spectral resolution of 0.5 nm for HITEMP. The~~ upper part of this table is adapted from Lampel et al. (2015b). This data is visualized in Figure 11.

Name		W0	W1	W2	**W3**	W4
Start of interval	[nm]	394.0	410.0	423.5	**434.0**	451.5
End of interval	[nm]	410.0	423.5	434.0	**451.5**	461.5
POKAZATEL		1.2605(6)	1.7052(13)	[0.8135(41)]	**1**	[2.1270(81)]

Table 7. Measured relative absorption band strengths for the different cross-sections with respect to the absorption at W3, the 7ν polyad, column in bold face. Errors obtained from the linear regression are shown for the last digits in brackets. The relative DOAS fit errors are listed in Table 8. Results with typical DOAS fit errors of more than 25% of the measured values were put in square brackets. MAX-DOAS values are corrected by the results of radiative transfer modelling (Lampel et al., 2015b).

[%]		W0	W1	W2	**W3**	W4
Start of interval	[nm]	394.0	410.0	423.5	**434.0**	451.5
End of interval	[nm]	410.0	423.5	434.0	**451.5**	461.5
POKAZATEL	MAX-DOAS	4	6	40	**0.8**	29

Table 8. Typical relative DOAS fit errors in fitting windows W0-W4 at a water vapour dSCD in W3 of 4×10^{23} molec cm^{-2} for an individual spectrum integrated over 60 s. Values are given in % and are corrected by the relative magnitudes given in Table 7.

During M91, for O$_4$ dSCDs an increase of about 5% was observed when including the additional absorption in the DOAS analysis. Thus, the water vapour absorption cannot explain the much larger correction factor for O$_4$ dSCDs introduced in various publications (it rather increases the observed discrepancies).

For HONO the water vapour absorption explains negative HONO dSCDs of several 10^{14} molec cm^{-2} for mid-latitude absolute water vapour volume mixing ratios. Negative HONO dSCD at low elevation angles were often observed around noon during the SOPRAN M91 campaign in the Peruvian upwelling when not considering water vapour absorption. In the same way negative OClO dSCDs in MAX-DOAS observations at low elevation angles of around -1×10^{13} molec cm^{-2} during M91 could also be linked to water vapour absorption at 363 nm.

Future DOAS evaluations encompassing the spectral range around 363 nm will require to include this water vapour absorption features, if they aim at residual spectra with an RMS of less than 4×10^{-4} or try to fit absorbers with measurement errors corresponding to optical densities of less than 1×10^{-3} in mid-latitude to tropical regions.

The predictions of *POKAZATEL* do not yield complete agreement with the observed absorption features. While, as discussed above, this line list should give very accurate line positions, the situation regarding absorption intensities is more problematic. This is indeed observed in the measurements presented here, as the position of the absorption is found to be accurate (shift of 0.02 ± 0.06 nm, or 1.5 ± 4.6 cm^{-1}), while the magnitude of the observed absorption bands differs relative to each other. This was before also observed in the blue spectral range by Lampel et al. (2015b). While the *ab initio* dipole moment calculations of Lodi et al. (2011) cover an appropriate range of geometries and are expected to be accurate, using them to construct a reliable DMS is not straightforward. A number of studies (Schwenke and Partridge, 2000; Lodi et al., 2008; Tennyson, 2014) have shown that it is difficult to produce analytic fits which correctly reproduce the intensity of weak transitions. Here we are dealing with very weak water absorptions on the margins of detectability. For this reason we performed some test calculations using the *POKAZATEL* methodology but utilizing the CVR DMS of Lodi et al. (2008). The results shown in subsection 4.3 indicate that this DMS (Lodi et al., 2008) could explain the systematic underestimation of the magnitude of water vapour absorption, but probably do not predict the spectral shape of the absorption peak as accurately as *POKAZATEL*. Further work is required on the precise representation of the *ab initio* DMS to try to resolve these problems. Studies should

also be performed to obtain a more reliable representation of the water dipole moment for the purpose of predicting absorption intensities in the near UV. Laboratory studies on this problem would also be very helpful.

The values for the absorption cross section of water vapour in the UV range reported by Du et al. (2013) cannot be confirmed. We derived upper limits, which are at least two orders of magnitude smaller in the spectral range from 310–370 nm.

5 ## 6 ~~Relative absorption strengths~~

~~Name W0 W1 W2 **W3** W4 Start of interval nm394.0 410.0 423.5 **434.0** 451.5 End of interval nm410.0 423.5 434.0 **451.5** 461.5~~

~~1.2605(6) 1.7052(13) 0.8135(41)**1** 2.1270(81)~~

~~Measured relative absorption band strengths for the different cross-sections with respect to the absorption at W3, the 7ν~~
10 ~~polyad, column in bold face. Errors obtained from the linear regression are shown for the last digits in brackets. The relative DOAS fit errors are listed in . Results with typical DOAS fit errors of more than 25% of the measured values were put in square brackets. MAX-DOAS values are corrected by the results of radiative transfer modelling Lampel et al. (2015b).~~

~~%W0 W1 W2 **W3** W4 Start of interval nm394.0 410.0 423.5 **434.0** 451.5End of interval nm410.0 423.5 434.0 **451.5** 461.5 MAX-DOAS 4 6 40 **0.8** 29~~

15 ~~Typical relative DOAS fit errors in fitting windows W0-W5 at a water vapour dSCD in W3 of for an individual spectrum integrated over 60 s. Values are given in % and are corrected by the relative magnitudes given in .~~

References

Bange, H.: Surface Ocean - Lower Atmosphere Study (SOLAS) in the upwelling region off Peru - Cruise No.M91, DFG-Senatskommission fuer Ozeanographie, METEOR-Berichte, 91, 69pp, doi:10.2312/cr_m91, https://portal.geomar.de/metadata/leg/show/316029, 2013.

Barber, R. J., Tennyson, J., Harris, G. J., and Tolchenov, R. N.: A high-accuracy computed water line list, Monthly Notices of the Royal Astronomical Society, 368, 1087–1094, doi:10.1111/j.1365-2966.2006.10184.x, http://mnras.oxfordjournals.org/content/368/3/1087.abstract, 2006.

Beirle, S., Sihler, H., and Wagner, T.: Linearisation of the effects of spectral shift and stretch in DOAS analysis, Atmospheric Measurement Techniques, 6, 661–675, doi:10.5194/amt-6-661-2013, http://www.atmos-meas-tech.net/6/661/2013/, 2013.

Bobrowski, N., von Glasow, R., Aiuppa, A., Inguaggiato, S., Louban, I., Ibrahim, O. W., and Platt, U.: Reactive halogen chemistry in volcanic plumes, Journal of Geophysical Research: Atmospheres, 112, n/a–n/a, doi:10.1029/2006JD007206, http://dx.doi.org/10.1029/2006JD007206, 2007.

Bobrowski, N., Kern, C., Platt, U., Hörmann, C., and Wagner, T.: Novel SO_2 spectral evaluation scheme using the 360-390 nm wavelength range, Atmospheric Measurement Techniques, 3, 879–891, doi:10.5194/amt-3-879-2010, http://www.atmos-meas-tech.net/3/879/2010/, 2010.

Bogumil, K., Orphal, J., Homann, T., Voigt, S., Spietz, P., Fleischmann, O., Vogel, A., Hartmann, M., Bovensmann, H., Frerik, J., and Burrows, J.: Measurements of Molecular Absorption Spectra with the SCIAMACHY Pre-Flight Model: Instrument Characterization and Reference Data for Atmospheric Remote-Sensing in the 230-2380nm Region., J. Photochem. Photobiol. A., 157, 167–184, 2003.

Boyarkin, O. V., Koshelev, M. A., Aseev, O., Maksyutenko, P., Rizzo, T. R., Zobov, N. F., Lodi, L., Tennyson, J., and Polyansky, O. L.: Accurate bond dissociation energy of water determined by triple-resonance vibrational spectroscopy and ab initio calculations, Chem. Phys. Lett., 568-569, 14–20, 2013.

Bussemer, M.: Der Ring- Effekt: Ursachen und Einfluß auf die spektroskopische Messung stratosphärischer Spurenstoffe, Diploma thesis, Heidelberg University, Heidelberg, Germany, 1993.

Chance, K. and Kurucz, R.: An improved high-resolution solar reference spectrum for earth's atmosphere measurements in the ultraviolet, visible, and near infrared, Journal of Quantitative Spectroscopy and Radiative Transfer, 111, 1289 – 1295, doi:http://dx.doi.org/10.1016/j.jqsrt.2010.01.036, special Issue Dedicated to Laurence S. Rothman on the Occasion of his 70th Birthday., 2010.

Chance, K. and Orphal, J.: Revised ultraviolet absorption cross sections of H_2CO for the HITRAN database, Journal of Quantitative Spectroscopy and Radiative Transfer, 112, 1509 – 1510, doi:10.1016/j.jqsrt.2011.02.002, 2011.

Clémer, K., Van Roozendael, M., Fayt, C., Hendrick, F., Hermans, C., Pinardi, G., Spurr, R., Wang, P., and De Mazière, M.: Multiple wavelength retrieval of tropospheric aerosol optical properties from MAXDOAS measurements in Beijing, Atmospheric Measurement Techniques, 3, 863–878, doi:10.5194/amt-3-863-2010, http://www.atmos-meas-tech.net/3/863/2010/, 2010.

Császár, A. G., Mátyus, E., Lodi, L., Zobov, N. F., Shirin, S. V., Polyansky, O. L., and Tennyson, J.: Ab initio prediction and partial characterization of the vibrational states of water up to dissociation, J. Quant. Spec. and Rad. Transf., 111, 1043–1064, 2010.

Deutschmann, T., Beirle, S., Friess, U., Grzegorski, M., Kern, C., Kritten, L., Platt, U., Prados-Roman, C., Pukīte, J., Wagner, T., Werner, B., and Pfeilsticker, K.: The Monte Carlo atmospheric radiative transfer model McArtim: Introduction and validation of Jacobians and 3D features, Journal of Quantitative Spectroscopy and Radiative Transfer, 112, 1119 – 1137, doi:http://dx.doi.org/10.1016/j.jqsrt.2010.12.009, 2011.

Donovan, A., Tsanev, V., Oppenheimer, C., and Edmonds, M.: Reactive halogens (BrO and OClO) detected in the plume of Soufrière Hills Volcano during an eruption hiatus, Geochemistry, Geophysics, Geosystems, 15, 3346–3363, doi:10.1002/2014GC005419, http://dx.doi.org/10.1002/2014GC005419, 2014.

Du, J., Huang, L., Min, Q., and Zhu, L.: The influence of water vapor absorption in the 290-350nm region on solar radiance: Laboratory studies and model simulation, Geophysical Research Letters, 40, 4788–4792, doi:10.1002/grl.50935, http://dx.doi.org/10.1002/grl.50935, 2013.

Dupré, P., Gherman, T., Zobov, N. F., Tolchenov, R. N., and Tennyson, J.: Continuous-wave cavity ringdown spectroscopy of the 8ν polyad of water in the 25 195 - 25 340 cm range, The Journal of chemical physics, 123, 154 307, 2005.

Eger, P.: Improving Long-Path DOAS measurements with a Laser Driven Light Source and a new fibre configuration, Masters thesis, Institut für Umweltphysik, Universität Heidelberg, 2014.

Fleischmann, O.: New ultraviolet absorption cross-sections of BrO at atmospheric temperatures measured by time-windowing Fourier transform spectroscopy, Journal of Photochemistry and Photobiology A: Chemistry, 168, 117–132, 2004.

Frieß U., Monks, P. S., Remedios, J. J., Rozanov, A., Sinreich, R., Wagner, T., and Platt, U.: MAX-DOAS O_4 measurements: A new technique to derive information on atmospheric aerosols: 2. Modeling studies, Journal of Geophys. Res., 111, D14203, doi: 10.1029/2005JD006 618, 2006.

General, S., Bobrowski, N., Pöhler, D., Weber, K., Fischer, C., and Platt, U.: Airborne I-DOAS measurements at Mt. Etna: BrO and {OClO} evolution in the plume, Journal of Volcanology and Geothermal Research, 300, 175 – 186, doi:http://dx.doi.org/10.1016/j.jvolgeores.2014.05.012, http://www.sciencedirect.com/science/article/pii/S0377027314001541, 2015.

Gliß, J., Bobrowski, N., Vogel, L., Pöhler, D., and Platt, U.: OClO and BrO observations in the volcanic plume of Mt. Etna - implications on the chemistry of chlorine and bromine species in volcanic plumes, Atmospheric Chemistry and Physics, 15, 5659–5681, doi:10.5194/acp-15-5659-2015, http://www.atmos-chem-phys.net/15/5659/2015/, 2015.

Grainger, J. and Ring, J.: Anomalous Fraunhofer line profiles, Nature, 193, 762, 1962.

Greenblatt, G. D., Orlando, J. J., Burkholder, J. B., and Ravishankara, A. R.: Absorption Measurements of Oxygen between 330 and 1140 nm, J. Geophys. Res., 95, 18 577–18 582, 1990.

Großmann, K., Frieß, U., Peters, E., Wittrock, F., Lampel, J., Yilmaz, S., Tschritter, J., Sommariva, R., von Glasow, R., Quack, B., Krüger, K., Pfeilsticker, K., and Platt, U.: Iodine monoxide in the Western Pacific marine boundary layer, Atmospheric Chemistry and Physics, 13, 3363–3378, doi:10.5194/acp-13-3363-2013, http://www.atmos-chem-phys.net/13/3363/2013/, 2013.

Hendrick, F., Müller, J.-F., Clémer, K., Wang, P., De Mazière, M., Fayt, C., Gielen, C., Hermans, C., Ma, J. Z., Pinardi, G., Stavrakou, T., Vlemmix, T., and Van Roozendael, M.: Four years of ground-based MAX-DOAS observations of HONO and NO_2 in the Beijing area, Atmospheric Chemistry and Physics, 14, 765–781, doi:10.5194/acp-14-765-2014, http://www.atmos-chem-phys.net/14/765/2014/, 2014.

Hermans, C., Vandaele, A. C., Carleer, M., Fally, S., Colin, R., Jenouvrier, A., Coquart, B., and Mérienne, M.-F.: Absorption Cross-Sections of Atmospheric Constituents: NO_2, O_2, and H_2O, Environ. Sci. & Pollut. Res., 6, 151–158, doi:10.1007/BF02987620, http://dx.doi.org/10.1007/BF02987620, 1999.

Hermans, C., Vandaele, A., Fally, S., Carleer, M., Colin, R., Coquart, B., Jenouvrier, A., and Merienne, M.-F.: Absorption cross-section of the collision-induced bands of oxygen from the UV to the NIR, in: Weakly interacting molecular pairs: unconventional absorbers of radiation in the atmosphere, pp. 193–202, Springer, 2003.

Hönninger, G. and Platt, U.: Observations of BrO and its vertical distribution during surface ozone depletion at Alert, Atmospheric Environment, 36, 2481–2489, 2002.

37

Hönninger, G., Friedeburg, C., and Platt, U.: Multi Axis Differential Absorption Spectroscopy (MAX-DOAS), Atmos. Chem. Phys., 4, 231–245, 2004.

Hörmann, C., Sihler, H., Bobrowski, N., Beirle, S., Penning de Vries, M., Platt, U., and Wagner, T.: Systematic investigation of bromine monoxide in volcanic plumes from space by using the GOME-2 instrument, Atmospheric Chemistry and Physics, 13, 4749–4781, doi:10.5194/acp-13-4749-2013, http://www.atmos-chem-phys.net/13/4749/2013/, 2013.

Irie, H., Nakayama, T., Shimizu, A., Yamazaki, A., Nagai, T., Uchiyama, A., Zaizen, Y., Kagamitani, S., and Matsumi, Y.: Evaluation of MAX-DOAS aerosol retrievals by coincident observations using CRDS, lidar, and sky radiometer in Tsukuba, Japan, Atmospheric Measurement Techniques, 8, 2775–2788, doi:10.5194/amt-8-2775-2015, http://www.atmos-meas-tech.net/8/2775/2015/, 2015.

Jacquinet-Husson, N., Scott, N., Chédin, A., Crépeau, L., Armante, R., Capelle, V., Orphal, J., Coustenis, A., Boonne, C., Poulet-Crovisier, N., et al.: The GEISA spectroscopic database: Current and future archive for Earth and planetary atmosphere studies, Journal of Quantitative Spectroscopy and Radiative Transfer, 109, 1043–1059, 2008.

Kattner, G.: The expedition of the research vessel "Polarstern" to the Antarctic in 2011/12 (ANT-XXVIII/2), http://hdl.handle.net/10013/epic.39675, 2012.

Kleffmann, J. and Wiesen, P.: Technical Note: Quantification of interferences of wet chemical HONO LOPAP measurements under simulated polar conditions, Atmospheric Chemistry and Physics, 8, 6813–6822, doi:10.5194/acp-8-6813-2008, http://www.atmos-chem-phys.net/8/6813/2008/, 2008.

Kraus, S.: DOASIS - A Framework Design for DOAS, Dissertation, Heidelberg University, https://comviswiki.iwr.uni-heidelberg.de/publications/dip/2006/Kraus_PhD2006.pdf, 2006.

Kühl, S., Pukīte, J., Deutschmann, T., Platt, U., and Wagner, T.: SCIAMACHY limb measurements of NO_2, BrO and OClO. Retrieval of vertical profiles: Algorithm, first results, sensitivity and comparison studies, Advances in Space Research, 42, 1747 – 1764, doi:http://dx.doi.org/10.1016/j.asr.2007.10.022, 2008.

Lampel, J.: Measurements of reactive trace gases in the marine boundary layer using novel DOAS methods, Dissertation, Institut für Umweltphysik, Heidelberg University, http://www.ub.uni-heidelberg.de/archiv/17394, 2014.

Lampel, J., Frieß, U., and Platt, U.: The impact of vibrational Raman scattering of air on DOAS measurements of atmospheric trace gases, Atmospheric Measurement Techniques, 8, 3767–3787, doi:10.5194/amt-8-3767-2015, http://www.atmos-meas-tech.net/8/3767/2015/, 2015a.

Lampel, J., Pöhler, D., Tschritter, J., Frieß, U., and Platt, U.: On the relative absorption strengths of water vapour in the blue wavelength range, Atmospheric Measurement Techniques, 8, 4329–4346, doi:10.5194/amt-8-4329-2015, http://www.atmos-meas-tech.net/8/4329/2015/, 2015b.

Lodi, L. and Tennyson, J.: Line lists for $H_2{}^{18}O$ and $H_2{}^{17}O$ based on empirically-adjusted line positions and ab initio intensities, J. Quant. Spec. and Rad. Transf., 113, 850–858, 2012.

Lodi, L., Tolchenov, R. N., Tennyson, J., Lynas-Gray, A., Shirin, S. V., Zobov, N. F., Polyansky, O. L., Császár, A. G., van Stralen, J. N., and Visscher, L.: A new ab initio ground-state dipole moment surface for the water molecule, The Journal of chemical physics, 128, 044 304, 2008.

Lodi, L., Tennyson, J., and Polyansky, O. L.: A global, high accuracy ab initio dipole moment surface for the electronic ground state of the water molecule, J. Chem. Phys, 135, 034 113, 2011.

Mahajan, A. S., Prados-Roman, C., Hay, T. D., Lampel, J., Pöhler, D., Großmann, K., Tschritter, J., Frieß, U., Platt, U., Johnston, P., Kreher, K., Wittrock, F., Burrows, J. P., Plane, J. M., and Saiz-Lopez, A.: Glyoxal observations in the global marine boundary layer, Journal of Geophysical Research: Atmospheres, 119, 6160–6169, doi:10.1002/2013JD021388, http://dx.doi.org/10.1002/2013JD021388, 2014.

Maksyutenko, P., Muenter, J. S., Zobov, N. F., Shirin, S. V., Polyansky, O. L., Rizzo, T. R., and Boyarkin, O. V.: Approaching the full set of energy levels of water, Journal of Chemical Physics, 126, 241 101–241 101, 2007.

Maksyutenko, P., Grechko, M., Rizzo, T. R., and Boyarkin, O. V.: State-resolved spectroscopy of high vibrational levels of water up to the dissociative continuum, Philosophical Transactions of the Royal Society A: Mathematical, Physical and Engineering Sciences, 370, 2710–2727, 2012.

Marquard, L. C., Wagner, T., and Platt, U.: Improved air mass factor concepts for scattered radiation differential optical absorption spectroscopy of atmospheric species, J. Geophys. Res., 105, 1315–1327, 2000.

Myhre, G., Shindell, D., Bréon, F.-M., Collins, W., Fuglestvedt, J., Huang, J., Koch, D., Lamarque, J.-F., Lee, D., Mendoza, B., Nakajima, T., Robock, A., Stephens, G., Takemura, T., and Zhang, H.: Anthropogenic and natural radiative forcing, in: Climate Change 2013: The Physical Science Basis. Contribution of Working Group I to the Fifth Assessment Report of the Intergovernmental Panel on Climate Change, edited by Stocker, T., Qin, D., Plattner, G.-K., Tignor, M., Allen, S., Boschung, J., Nauels, A., Xia, Y., Bex, V., and Midgley, P., pp. 659–740, Cambridge University Press, Cambridge, United Kingdom and New York, NY, USA, doi:10.1017/CBO9781107415324.018, 2013.

Naggar, S. E. D. E.: The expedition of the research vessel "Polarstern" to the Antarctic in 2011 (ANT-XXVIII/1), http://hdl.handle.net/10013/epic.40417, 2012.

Oetjen, H., Wittrock, F., Richter, A., Chipperfield, M. P., Medeke, T., Sheode, N., Sinnhuber, B.-M., Sinnhuber, M., and Burrows, J. P.: Evaluation of stratospheric chlorine chemistry for the Arctic spring 2005 using modelled and measured OClO column densities, Atmospheric Chemistry and Physics, 11, 689–703, doi:10.5194/acp-11-689-2011, http://www.atmos-chem-phys.net/11/689/2011/, 2011.

Ortega, I., Berg, L. K., Ferrare, R. A., Hair, J. W., Hostetler, C. A., and Volkamer, R.: Elevated aerosol layers modify the O2-O2 absorption measured by ground-based MAX-DOAS, Journal of Quantitative Spectroscopy and Radiative Transfer, 176, 34 – 49, doi:http://dx.doi.org/10.1016/j.jqsrt.2016.02.021, http://www.sciencedirect.com/science/article/pii/S0022407315301746, 2016.

Partridge, H. and Schwenke, D. W.: The determination of an accurate isotope dependent potential energy surface for water from extensive ab initio calculations and experimental data, J. Chem. Phys, 106, 4618–4639, 1997.

Perner, D. and Platt, U.: Detection of Nitrous Acid in the Atmosphere by Differential OpticalAbsorption, Geophys. Res. Lett., 6, 917–920, 1979.

Peters, E., Wittrock, F., Richter, A., Alvarado, L. M. A., Rozanov, V. V., and Burrows, J. P.: Liquid water absorption and scattering effects in DOAS retrievals over oceans, Atmospheric Measurement Techniques, 7, 4203–4221, doi:10.5194/amt-7-4203-2014, http://www.atmos-meas-tech.net/7/4203/2014/, 2014.

Pfeilsticker, K., Bösch, H., Camy-Peyret, C., Fitzenberger, R., Harder, H., and Osterkamp, H.: First atmospheric profile measurements of UV/visible O4 absorption band intensities: Implications for the spectroscopy, and the formation enthalpy of the O2-O2 dimer, Geophysical Research Letters, 28, 4595–4598, doi:10.1029/2001GL013734, http://dx.doi.org/10.1029/2001GL013734, 2001.

Pinardi, G., Van Roozendael, M., Abuhassan, N., Adams, C., Cede, A., Clémer, K., Fayt, C., Frieß, U., Gil, M., Herman, J., Hermans, C., Hendrick, F., Irie, H., Merlaud, A., Navarro Comas, M., Peters, E., Piters, A. J. M., Puentedura, O., Richter, A., Schönhardt, A., Shaiganfar, R., Spinei, E., Strong, K., Takashima, H., Vrekoussis, M., Wagner, T., Wittrock, F., and Yilmaz, S.: MAX-DOAS formaldehyde

slant column measurements during CINDI: intercomparison and analysis improvement, Atmospheric Measurement Techniques, 6, 167, doi:10.5194/amt-6-167-2013, http://www.atmos-meas-tech.net/6/167/2013/, 2013.

Platt, U. and Stutz, J.: Differential optical absorption spectroscopy, Springer, Berlin, Heidelberg, 2008.

Platt, U., Marquard, L., Wagner, T., and Perner, D.: Corrections for Zenith Scattered Light DOAS, Geophys. Res. Letters, 24, 1759–1762, 1997.

Pöhler, D., Vogel, L., Frieß U., and Platt, U.: Observation of halogen species in the Amundsen Gulf, Arctic, by active long-path differential optical absorption spectroscopy, Proceedings of the National Academy of Sciences, 107, 6582–6587, doi:10.1073/pnas.0912231107, http://www.pnas.org/content/107/15/6582.abstract, 2010.

Polyansky, O. L., Kyuberis, A. A., Lodi, L., Tennyson, J., Ovsyannikov, R. I., and Zobov, N.: ExoMol molecular line lists XX: high accuracy computed line list for hot $H_2^{16}O$, Mon. Not. R. Astron. Soc., 2016.

Pukīte, Janis, J., Kühl, S., Deutschmann, T., Platt, U., and Wagner, T.: Extending differential optical absorption spectroscopy for limb measurements in the UV, Atmospheric Measurement Techniques, 3, 631–653, doi:10.5194/amt-3-631-2010, http://www.atmos-meas-tech.net/3/631/2010/, 2010.

Regalia, L., Oudot, C., Mikhailenko, S., Wang, L., Thomas, X., Jenouvrier, A., and Von der Heyden, P.: Water vapor line parameters from 6450 to 9400 cm^{-1}, J. Quant. Spec. and Rad. Transf., 136, 119–136, 2014.

Richter, A., Wittrock, F., Ladstätter-Weißenmayer, A., and Burrows, J.: GOME measurements of stratospheric and tropospheric BrO, Advances in Space Research, 29, 1667 – 1672, doi:http://dx.doi.org/10.1016/S0273-1177(02)00123-0, 2002.

Rothman, L., Gordon, I., Barbe, A., Benner, D., Bernath, P., Birk, M., Boudon, V., Brown, L., Campargue, A., Champion, J.-P., Chance, K., Coudert, L., Dana, V., Devi, V., Fally, S., Flaud, J.-M., Gamache, R., Goldman, A., Jacquemart, D., Kleiner, I., Lacome, N., Lafferty, W., Mandin, J.-Y., Massie, S., Mikhailenko, S., Miller, C., Moazzen-Ahmadi, N., Naumenko, O., Nikitin, A., Orphal, J., Perevalov, V., Perrin, A., Predoi-Cross, A., Rinsland, C., Rotger, M., Šimečková, M., Smith, M., Sung, K., Tashkun, S., Tennyson, J., Toth, R., Vandaele, A., and Auwera, J. V.: The HITRAN 2008 molecular spectroscopic database, Journal of Quantitative Spectroscopy and Radiative Transfer, 110, 533–572, doi:http://dx.doi.org/10.1016/j.jqsrt.2009.02.013, 2009.

Rothman, L., Gordon, I., Barber, R., Dothe, H., Gamache, R., Goldman, A., Perevalov, V., Tashkun, S., and Tennyson, J.: HITEMP, the high-temperature molecular spectroscopic database, Journal of Quantitative Spectroscopy and Radiative Transfer, 111, 2139 – 2150, doi:10.1016/j.jqsrt.2010.05.001, xVIth Symposium on High Resolution Molecular Spectroscopy (HighRus-2009), 2010.

Rothman, L., Gordon, I., Babikov, Y., Barbe, A., Benner, D. C., Bernath, P., Birk, M., Bizzocchi, L., Boudon, V., Brown, L., Campargue, A., Chance, K., Cohen, E., Coudert, L., Devi, V., Drouin, B., Fayt, A., Flaud, J.-M., Gamache, R., Harrison, J., Hartmann, J.-M., Hill, C., Hodges, J., Jacquemart, D., Jolly, A., Lamouroux, J., Roy, R. L., Li, G., Long, D., Lyulin, O., Mackie, C., Massie, S., Mikhailenko, S., Müller, H., Naumenko, O., Nikitin, A., Orphal, J., Perevalov, V., Perrin, A., Polovtseva, E., Richard, C., Smith, M., Starikova, E., Sung, K., Tashkun, S., Tennyson, J., Toon, G., Tyuterev, V., and Wagner, G.: The HITRAN2012 molecular spectroscopic database, Journal of Quantitative Spectroscopy and Radiative Transfer, 130, 4 – 50, doi:http://dx.doi.org/10.1016/j.jqsrt.2013.07.002, hITRAN2012 special issue, 2013.

Saiz-Lopez, A. and von Glasow, R.: Reactive halogen chemistry in the troposphere, Chem. Soc. Rev., 41, 6448–6472, doi:10.1039/C2CS35208G, http://dx.doi.org/10.1039/C2CS35208G, 2012.

Sansonetti, C. J., Salit, M. L., and Reader, J.: Wavelengths of spectral lines in mercury pencil lamps, Appl. Opt., 35, 74–77, doi:10.1364/AO.35.000074, http://ao.osa.org/abstract.cfm?URI=ao-35-1-74, 1996.

Schwenke, D. W. and Partridge, H.: Convergence testing of the analytic representation of an ab initio dipole moment function for water: improved fitting yields improved intensities, The Journal of Chemical Physics, 113, 6592–6597, 2000.

Serdyuchenko, A., Gorshelev, V., Weber, M., Chehade, W., and Burrows, J. P.: High spectral resolution ozone absorption cross-sections - Part 2: Temperature dependence, Atmospheric Measurement Techniques, 7, 625–636, doi:10.5194/amt-7-625-2014, http://www.atmos-meas-tech.net/7/625/2014/, 2014.

Shefov, N. N.: Intensivnosti nokotorykh emissiy sumerochnogo i nochnogo neba (Intensities of some Emissions of the Twilight and Night Sky), Spectral, electrophotometrical and radar researches of aurorae and airglow, IGY program, section IV, 1, 25, 1959.

Smirnov, A., Holben, B. N., Slutsker, I., Giles, D. M., McClain, C. R., Eck, T. F., Sakerin, S. M., Macke, A., Croot, P., Zibordi, G., Quinn, P. K., Sciare, J., Kinne, S., Harvey, M., Smyth, T. J., Piketh, S., Zielinski, T., Proshutinsky, A., Goes, J. I., Nelson, N. B., Larouche, P., Radionov, V. F., Goloub, P., Krishna Moorthy, K., Matarrese, R., Robertson, E. J., and Jourdin, F.: Maritime Aerosol Network as a component of Aerosol Robotic Network, Journal of Geophysical Research: Atmospheres, 114, doi:10.1029/2008JD011257, http://dx.doi.org/10.1029/2008JD011257, 2009.

Solomon, S., Mount, H. G., Sanders, R. W., and Schmeltekopf, A. L.: Visible spectroscopy at McMurdo station, Antarctica 2. Observations of OClO, J. Geophys. Res., 92, 8329–8338, 1987.

Spinei, E., Cede, A., Herman, J., Mount, G. H., Eloranta, E., Morley, B., Baidar, S., Dix, B., Ortega, I., Koenig, T., and Volkamer, R.: Ground-based direct-sun DOAS and airborne MAX-DOAS measurements of the collision-induced oxygen complex, O_2O_2, absorption with significant pressure and temperature differences, Atmospheric Measurement Techniques, 8, 793–809, doi:10.5194/amt-8-793-2015, http://www.atmos-meas-tech.net/8/793/2015/, 2015.

Stutz, J. and Platt, U.: Numerical Analysis and Estimation of the Statistical Error of Differential Optical Absorption Spectroscopy Measurements with Least-Squares methods, Appl. Opt., 35, 6041–6053, 1996.

Stutz, J., Kim, E. S., Platt, U., Bruno, P., Perrino, C., and Febo, A.: UV-visible Absorption Cross-Section of Nitrous Acid, J. Geophys. Res., 105, 14 585–14 592, 1999.

Tennyson, J.: Vibration–rotation transition dipoles from first principles, Journal of Molecular Spectroscopy, 298, 1–6, 2014.

Tennyson, J. and Yurchenko, S. N.: ExoMol: molecular line lists for exoplanet and other atmospheres, Monthly Notices of the Royal Astronomical Society, 425, 21–33, 2012.

Tennyson, J., Kostin, M. A., Barletta, P., Harris, G. J., Polyansky, O. L. ., Ramanlal, J., and Zobov, N. F.: DVR3D: a program suite for the calculation of rotation-vibration spectra of triatomic molecules, Comput. Phys. Commun., 163, 85–116, 2004.

Tennyson, J., Bernath, P. F., Brown, L. R., Campargue, A., Carleer, M. R., Császár, A. G., Daumont, L., Gamache, R. R., es, J. T. H., Naumenko, O. V., Polyansky, O. L., Rothmam, L. S., Vandaele, A. C., Zobov, N. F., Al Derzi, A. R., Fábri, C., Fazliev, A. Z., rtenbacher, T. F., Gordon, I. E., Lodi, L., and Mizus, I. I.: IUPAC critical evaluation of the rotational-vibrational spectra of wat er vapor. Part III. Energy levels and transition wavenumbers for $H_2{}^{16}O$, J. Quant. Spec. and Rad. Transf., 117, 29–80, 2013.

Thalman, R. and Volkamer, R.: Temperature dependent absorption cross-sections of O_2–O_2 collision pairs between 340 and 630 nm and at atmospherically relevant pressure, Physical Chemistry Chemical Physics, 15, 15 371–15 381, doi:10.1039/C3CP50968K, http://dx.doi.org/10.1039/C3CP50968K, 2013.

Theys, N., De Smedt, I., Van Roozendael, M., Froidevaux, L., Clarisse, L., and Hendrick, F.: First satellite detection of volcanic OClO after the eruption of Puyehue-Cordon Caulle, Geophysical Research Letters, 41, 667–672, doi:10.1002/2013GL058416, http://dx.doi.org/10.1002/2013GL058416, 2014.

41

Vandaele, A., Hermans, C., Simon, P., Carleer, M., Colin, R., Fally, S., Merienne, M., Jenouvrier, A., and Coquart, B.: Measurements of the NO_2 absorption cross-section from $42\,000\,cm^{-1}$ to $10\,000\,cm^{-1}$ (238-1000 nm) at 220 K and 294 K, Journal of Quantitative Spectroscopy and Radiative Transfer, 59, 171 – 184, doi:10.1016/S0022-4073(97)00168-4, atmospheric Spectroscopy Applications 96, 1998.

Vandaele, A. C., Hermans, C., and Fally, S.: Fourier transform measurements of SO 2 absorption cross sections: II.: Temperature dependence in the 29000–44000cm- 1 (227–345nm) region, Journal of Quantitative Spectroscopy and Radiative Transfer, 110, 2115–2126, 2009.

Vogel, L., Sihler, H., Lampel, J., Wagner, T., and Platt, U.: Retrieval interval mapping: a tool to visualize the impact of the spectral retrieval range on differential optical absorption spectroscopy evaluations, Atmospheric Measurement Techniques, 6, 275–299, doi:10.5194/amt-6-275-2013, http://www.atmos-meas-tech.net/6/275/2013/, 2013.

Voigt, S., Orphal, J., Bogumil, K., and Burrows, J. P.: The temperature dependence (203-293K) of the absorption cross sections of O_3 in the 230-850nm region measured by Fourier-transform spectroscopy, J. of Photochemistry and Photobiology A, 143, 1–9, 2001.

Volkamer, R., Baidar, S., Campos, T. L., Coburn, S., DiGangi, J. P., Dix, B., Eloranta, E. W., Koenig, T. K., Morley, B., Ortega, I., Pierce, B. R., Reeves, M., Sinreich, R., Wang, S., Zondlo, M. A., and Romashkin, P. A.: Aircraft measurements of BrO, IO, glyoxal, NO_2, H_2O, O_2–O_2 and aerosol extinction profiles in the tropics: comparison with aircraft-/ship-based in situ and lidar measurements, Atmospheric Measurement Techniques, 8, 2121–2148, doi:10.5194/amt-8-2121-2015, http://www.atmos-meas-tech.net/8/2121/2015/, 2015.

Wagner, T., von Friedeburg, C., Wenig, M., Otten, C., and Platt, U.: UV-visible observations of atmospheric O_4 absorptions using direct moonlight and zenith-scattered sunlight for clear-sky and cloudy sky conditions, Journal of Geophysical Research: Atmospheres, 107, AAC 3–1–AAC 3–15, doi:10.1029/2001JD001026, http://dx.doi.org/10.1029/2001JD001026, 4424, 2002.

Wagner, T., Heland, J., Zöger, M., and Platt, U.: A fast H_2O total column density product from GOME–Validation with in-situ aircraft measurements, Atmospheric Chemistry and Physics, 3, 651–663, 2003.

Wagner, T., Dix, B., v. Friedeburg, C., Frieß, U., Sanghavi, S., Sinreich, R., and Platt, U.: MAX-DOAS O_4 measurements: A new technique to derive information on atmospheric aerosols - Principles and information content, J. Geophys. Res., 109, D22 205, 2004.

Wagner, T., Deutschmann, T., and Platt, U.: Determination of aerosol properties from MAX-DOAS observations of the Ring effect, Atmospheric Measurement Techniques, 2, 495–512, doi:10.5194/amt-2-495-2009, http://www.atmos-meas-tech.net/2/495/2009/, 2009.

Wagner, T., Andreae, M. O., Beirle, S., Dörner, S., Mies, K., and Shaiganfar, R.: MAX-DOAS observations of the total atmospheric water vapour column and comparison with independent observations, Atmospheric Measurement Techniques, 6, 131–149, doi:10.5194/amt-6-131-2013, http://www.atmos-meas-tech.net/6/131/2013/, 2013.

Wang, Y., Beirle, S., Hilboll, A., Jin, J., Kyuberis, A. A., Lampel, J., Li, A., Luo, Y., Lodi, L., Ma, J., Navarro, M., Ortega, I., Peters, E., Polyansky, O. L., Remmers, J., Richter, A., Rodriguez, O. P., Roozendael, M. V., Seyler, A., Tennyson, J., Volkamer, R., Xie, P., Zobov, N. F., and Wagner, T.: MAX-DOAS measurements of HONO slant column densities during the MAD-CAT campaign: inter-comparison and sensitivity studies on spectral analysis settings, Atmospheric Measurement Techniques, in preparation, 2016.

Wenig, M., Jähne, B., and Platt, U.: Operator representation as a new differential optical absorption spectroscopy formalism, Appl. Opt., 44, 3246–3253, doi:10.1364/AO.44.003246, http://ao.osa.org/abstract.cfm?URI=ao-44-16-3246, 2005.

Wilson, E. M., Wenger, J. C., and Venables, D. S.: Upper limits for absorption by water vapor in the near-UV, Journal of Quantitative Spectroscopy and Radiative Transfer, 170, 194 – 199, doi:http://dx.doi.org/10.1016/j.jqsrt.2015.11.015, http://www.sciencedirect.com/science/article/pii/S0022407315301618, 2016.

Wong, K. W., Tsai, C., Lefer, B., Haman, C., Grossberg, N., Brune, W. H., Ren, X., Luke, W., and Stutz, J.: Daytime HONO vertical gradients during SHARP 2009 in Houston, TX, Atmospheric Chemistry and Physics, 12, 635–652, doi:10.5194/acp-12-635-2012, http://www.atmos-chem-phys.net/12/635/2012/, 2012.

Dear editor, we like to thank the reviewers for their helpful comments, which we answer as detailled below.

The first review listed a number of minor revisions, while the second review suggested major revisions consisting of a larger number of revisions. We answered all of the listed points and answered some of the suggestions given in the respective introduction of the review. Finally we corrected the edited manuscript again.

(Numbers of equations, figures, lines and pages refer to the discussion manuscript, if not mentioned otherwise. **Authors' reponses are written in bold face**, the referees' text is shown in normal face.)

1 Referee #1

Lampel et al. report new experimental observations for water absorption bands below 390 nm and consider how this water absorption influences the retrieval of other atmospheric species in a spectral fit. Water absorption in the near-UV region has received significant attention in the last few years, notably with a report of significant water vapour absorption below 360 nm, contrary to theoretical predictions of decreasing water absorption strength at shorter wavelengths. That report has since been called into question, leaving no clear experimental evidence for water absorption at such short wavelengths, despite theoretical predications of several very weak absorption bands. Using very long optical pathlengths through the atmosphere in both LP-DOAS and MAX-DOAS measurements, Lampel et al. convincing verify a water absorption band around 363 nm, both through the strong correlation between this band and a much stronger, well attested water absorption at longer wavelengths, and through the excellent match with the expected band structure and position of the latest theoretical line list (POKAZATEL, 2016). Similar evidence was presented for another water absorption band at 376 nm, but other water bands (including a predicted band around 335 nm) could not be confirmed. The magnitude of predicted water absorption in the 363 nm and 376 nm bands was too low by a factor of 2 3. The focus of the paper then turns to the effect of the 363 nm water absorption band on the spectral analysis and quantification of other molecular species in the near-UV. These include O4, HONO, OClO, and SO2. The impact on water absorption on these retrievals is not large, but nonetheless significant enough to warrant inclusion in future retrievals for these long open path measurements. This is a comprehensive & multi-faceted study of water absorption in this spectral region and I have no particular concerns about the analysis and conclusions of the paper. The water absorption is confirmed in three distinct data sets with large differences in the water slant column densities. This approach is necessary given the small magnitude of water absorption in the experimental spectra. The authors take considerable pains to rule out other confounding factors in the spectral analysis, which include wavelengths shifts in the O4 band, differences between experimental and theoretical spectra. The effects of different atmospheric structure on radiative transfer are also simulated. These experimental and analytical results are internally consistent within the uncertainties of the measurement. What may be valuable for future work on radiative transfer and theoretical studies on the water molecule absorption, is some discussion in the paper of whether it is possible to obtain more detailed experimental measurements of water absorption lines in the near-UV. In particular, would such an analysis be possible and more sensitive with a higher resolution system? Moreover, much of the initial impetus for measur-

ing the water absorption spectrum was concerned with radiative transfer in the atmosphere. What implications does this paper bring to bear on that question? Possibly owing to the variety of topics explored, this is not an easy paper to read. Nevertheless, the standard of editing falls short of ACP standards and should be addressed. Some obvious errors are listed in the technical corrections, and I encourage the authors to review the text carefully again.

We would like to thank Referee #1 for the helpful comments. The comments helped us to improve the manuscript, showed up some missing details and improved the overall manuscript. We thank the reviewer for suggesting further points which could be studied in future studies. We agree that water vapour absorption in the blue and the UV needs further attention, in order to clarify the magnitude of currently known (and often used in various spectral retrievals, such as NO2 and IO) absorptions bands (see e.g. [Lampel et al., 2015]) as well as to quantify the magnitude of the absorptions in the UV. In view of the fact that the H2O lines are much narrower than our spectral resolution we agree with the suggestion of the reviewer that studies with higher spectral resolution could also be helpful. These measurements can ultimately also contribute further to the understanding of the water molecule which in turn will provide better models and thus better line lists. This step is then however clearly outside the scope of this manuscript.

Technical corrections:

1. Reported physical properties should have a space between the value and the units. This is not consistently adhered to in the manuscript.

   We corrected these formatting issues (which appeared mostly for the wave number values).

2. Reference needed: p.4, l.22 after 'unaccounted tropospheric absorber'

   We admit that this is a strong statement after various publications have used the O4 absorption in this spectral range. However, such a persistent residual structure can always point to 'unaccounted tropospheric absorber' if instrumental failures can be excluded, thus this is always a possibility. We split the sentence and the second part now reads: 'In any case, it could be possibly explained by an unaccounted tropospheric absorber'. We are not aware that this option was discussed in literature.

3. P.7, l.2-6: It is unclear whether the absorption cross section refers to total cross section, or to the differential cross section. The symbols used are those conventionally used for total absorption cross section. See e.g., Platt, Phys. Chem. Chem. Phys., 1999, 1, 5409-5415, for the usual description.

   We refer here to total cross-section and changed the text to make this clear.

4. P23, l18: Do the authors have an explanation for the residual feature observed in one dataset?

   We do not. However, as due to the almost constant humidity during M91 the dSCDs of O_4 and H_2O and maybe other absorbers with similar concentration height profiles, a clear connection to water vapour absorption

cannot be established for this dataset. Therefore we concluded that this is not necessarily connected to water vapour absorption.

5. The quantities described in Table 5 are not sufficiently clear to this reviewer, and the columns should be more precisely defined than 'impact'. If, as I presume, what is meant is (e.g.) the difference between RMS (water absorption included) RMS (no water absorption), then this should be stated. Likewise for the other properties.

   We added a short explanation to the caption of the figure.

6. The following parts of the document should be edited: Abstract: a. 'visible spectrum at a decreasing' . . . 'visible spectrum with decreasing'

   Corrected.

7. 'until its dissociation limit' . . . 'up to its dissociation limit'

   Corrected.

8. Page 1: a. 15: 'vapour. it plays a key role for the'. . .' vapour. It plays a key role in the'

   Corrected.

9. p1 16-17: 'Earth. . .absorption' . . .unclear.

   rewritten and shortened.

10. p1 19: 'also required assessing'. . .' also required for assessing'

    Corrected.

11. Page 4:19: 'and SO2 , potentially even HCHO and BrO'. Unclear

    Now we list all of the potentially affected trace gases, without weakening the statement for HCHO and BrO. This was written this way, as the water vapour absorption in the typical HCHO/BrO retrieval intervals could not be unambiguously identified in this publication.

12. Page 5: 20: 'Bremerhaven/. . ..employed'. Unclear

    We reorded and shortened this sentence to clarify it.

13. Page 7: a. 3: 'and narrow-band'. . .' and a narrow-band'

    Done.

14. b. 15: measurements is, that . . . measurements is that

    Done.

15. Page 8: a. 8: 'Longpath(LP)-DOAS' and 'here a a LASER-driven'

    Corrected.

16. 15: Unclear.

    This is an advantage compared to MAX-DOAS measurements, a statement to this was added to the text. MAX-DOAS measurements use scattered light

and therefore the light path length is initially not known and depends on a variety of factors, such as e.g. aerosol extinction profiles, viewing geometry and sun position.

17. Page 12:19: 'Due to need to'

    Corrected.

18. Page 14: 2: 'selected such according'. Unclear

    Reordered and clarified.

19. Page 21: 27: 'water cross-section of O3 ,'. . .' absorption cross-section of O3 ,'

    Corrected.

20. Page 29: 29: 'strenghts'

    Corrected.

2 Referee #2

The paper discusses important new information about water vapour absorption in the UV spectral region and its effects on DOAS retrievals. With this it presents important results which are suitable for publishing in ACP. However, the presentation is at many points confusing and I suggest publication only after major revisions. Due to the lengths of this paper of 40 pages the content is hard to follow and this isnt helped by the fact that section titles dont always fit the content (e.g. section 4.9 is about the accuracy of the wavelengths axis and this should be spelled out in the title; section 1.3 lists science questions and not an outline). Another problem is that the authors clearly have lost track themselves, e.g.: there is no proper introduction about the differences of HITRAN 2009, 2012, HITEMP, or BT2 in the beginning of the manuscript, but there are bits and pieces of information later on in the text; the lower panels in Figure 1 are not referred to in the text at all; the text refers to a figure 4.2 which I believe is actually Figure 6; on the other hand, there is no reference in the text to the right panel in Figure 4; the spectral resolution of the instruments is stated 3 times in the manuscript, but some important information is only listed in captions, e.g. how the upper limit is calculated for Table 4; there are 2 different symbols used for absorber concentrations in the equations. More details/corrections below. However, I would like to encourage the authors to give this manuscript a thorough read themselves and to restructure some of its content, especially double-checking if the information provided in the figures/tables and their captions is actually used and sufficiently described in the manuscript.

We would like to thank Referee #2 for the positive remarks on the scientific value of our manuscript and the numerous helpful comments. They helped us to improve the structure of the manuscript to correct some inconsistencies and to clarify some points. Together with the revisions made in response to the comments of reviewer #1 these changes amount to a major revision of our manuscript.

Points addressed in the introduction:

1. 1. There is no proper introduction about the differences of HITRAN 2009, 2012, HITEMP, or BT2 in the beginning of the manuscript, but there are bits and pieces of information later on in the text

We added a several more sentences and some more references in the introduction of HITRAN, HITEMP and BT2. We moved the text part about the intensity line cutoff to the introduction. The details of how the line lists were created can be found in the given references. We changed 'HITRAN 2009' to 'HITRAN 2008 version 2009' due to a suggestion by Iouli Gordon.

2. 2. the lower panels in Figure 1 are not referred to in the text at all

   We added these absorption cross-sections in order to illustrate the possibly affected spectral trace gas retrievals. We added a reference to this panel to the text when the potentially affected trace gas retrievals are listed..

3. 3. the text refers to a figure 4.2 which I believe is actually Figure 6;

   This is correct. Many thanks for this hint! The reason was a wrong interpretation of the label in latex by the autoref command. This is fixed and refers now to section 4.2.

4. 4. on the other hand, there is no reference in the text to the right panel in Figure 4;

   This is correct, as the text did not explicitly refer to the right panel. We added an explicit reference to this figure when the measurement error of the LPDOAS observations is discussed in the text.

5. 5. the spectral resolution of the instruments is stated 3 times in the manuscript, but some important information is only listed in captions, e.g. how the upper limit is calculated for Table 4

   We moved the description from the caption to the text. We mentioned the spectral resolution in Table 4, as it differs for both instruments.

6. 6. there are 2 different symbols used for absorber concentrations in the equations.

   This is fixed.

7. 7. section 4.9 is about the accuracy of the wavelengths axis and this should be spelled out in the title

   Section 4.9 is about the accuracy of the wavelengths axis as well as about the shape of the absorption structures. If these are not represented well enough in the absorption line list, residual structures could have been observed. Both of these aspects are treated in this paragraph. We renamed this section to 'Estimation of the accuracy of the shape and wavelength calibration of the POKAZATEL H_2O cross-section'

Specific comments:

1. p.1, l.5, 11, 13: 363 nm or 362.3 nm. I understand that the authors refer to the peak of the absorption and the feature in general. But using two different numbers without further explanation in the abstract is confusing.

   We changed this in the caption of Table 5, but left the 362.3nm value in the abstract unchanged as it describes the actual maximum of the absorption band at the given spectral resolution.

2. p.1, l.8: Add: For MAX-DOAS measurements, we observed. . .

   Added.

3. p.1, l.8: It correlates. . . refers to something like 2 months of data. That should be made clear at this point.

   A larger data set covering a longer time span could have been used, but it would not have changed the outcome of the study. We added 'The retrieved column densities from two months of measurement data and more than 2000 individual observations at different latitudes' to this sentence.

4. p.1, l.10: Add: . . .line intensities at 362.3 nm are underestimated by. . .

   We added the wavelength of the absorption band in order to avoid confusion.

5. p1., l.12: spectral retrievals

   Changed.

6. p.1, l.15: It

   Modified.

7. Figure 1, top panel: The y-axis on the inset plot seems to have a different extent, especially at the lower end. This makes it appear as if the POKAZATEL has more lines in that inset than in the large plot.

   Yes, the limits of the y-axis are different - at both sides. To avoid confusion, we added also labels to the inset plot.

8. p.3, l.6 and following: Why not refer to Figure 1 at this point already? The intro would read easier if you structured it like this: In Lampel et al. (2015b) you already suspected additional water vapour lines. But those could not be found in the line list available back then. Describe the available line list until then. Then you introduce the new POKAZATEL list and that this new information will be investigated with additional field measurements. Splitting the intro into subsections actually interrupts the flow of the argument.

   We moved the part about the observations in Lampel et al. (2015b) to the top of the page and refer to Fig. 1.

9. p.3, l.16-17: Add that those were lab measurements.

   Added.

10. p.3, l.20: structures in the spectral range

    'systematic residual structures' → 'systematic structures in the fit residuals'

11. p3., l.24: individual line cut-off: what is that?

    We added a reference to the HITEMP publication and added 'This cut-off removes weak absorption lines from the line list and was introduced for the HITRAN and HITEMP line lists to reduce the number of individual absorption lines for further processing as described e.g. in ... '

12. p.3, l.28-29: No new paragraph needed here

   Removed.

13. p.3, l.34: (in principle): Any explanation what this refers to or remove?

   Removed. Referred to the fact that these absorptions are not yet observed and verified, but this is clear from the context.

14. p.4, l.15: I would remove potential here

   Removed, added a reference to figure 1.

15. p.4, l.18,21: O4 was already used without being introduced as were the other species.

   We added the name for each trace gas, e.g. 'HCHO' → 'formaldehyde (HCHO)'

16. p.4, l.22: Please add reference for unaccounted tropospheric absorber.

   We're not aware of any publication which reported this. However, residual structures in the spectral retrievals can always point to potentially neglected absorbers. We split the sentence, the second part is now 'In any case, it could be possibly explained by an unaccounted tropospheric absorber'. See also our response to reviewer #1 on the same topic.

17. p.4, l.23-26: This statement at this point is difficult to understand for a person not very familiar with MAX-DOAS measurements and the corresponding radiative transfer. Either remove or give more explanation. See also below.

   Removed here as it can be explained more nicely in the section on data evaluation.

18. p.5, l.2: formatting: brackets should be within the sentence.

   Changed.

19. Section 2: Maybe add here that LP-DOAS is active and MAX-DOAS a passive technique

   We added passive and active to this section.

20. p.5, l.12: remove space after 15.

   Removed.

21. p.5, l.15: Full stop after 0.45nm.

   Added.

22. p.5, l.16: The latitudinal extent has nothing to do with variations of the water vapour mixing ration. Also, Figure 2 is misleading since the satellite in the background is from a different time than the M91 cruise.

   We agree that latitude and water vapour mixing ratio are per se independent, but the maximum absolute water vapour content of air depends strongly on temperature. Therefore strong latitudinal gradients in water vapour mixing ratio can be seen, e.g. during *ANT XXVIII/1-2* . We added that the cruise M91 was additionally also a short one, limiting the variation of observed water vapour mixing ratios.

23. p.5, l.17-19: S.a.

    Here we added an explanation about why O_4 and water vapour are correlated for measurement conditions with small variations in absolute humidity: 'The O_4 dSCD is as a first order approximation proportional to the effective light path length, the H_2O dSCD is proportional to the light path length as well, but also to the absolute humidity along the light path according to Eq. 2. '

24. p.5, l.20: therefore: s.a. water vapour changes because it changes and not because the measurements are at a different latitude.

    We removed 'therefore'.

25. p.5, l.22-24: Maybe make that 2-3 sentences. Your point that O4 and H2O absorb in similar region in the UV as well as in the visible doesnt fully come across. You could also refer to Figure 1 here.

    We split the sentences and referred again to figure 1.

26. p.5, l.3: lambda is not introduced

    We added a short introduction for the wavelength λ.

27. Figure 2: Its not clear how you get from a slant column ratio to a vertical column of one of the species. Also these results are not discussed in the manuscript.

    Figure 2 is intended to be an overview about the measurement locations. We added a short paragraph to the text: 'In Fig. 2 the ratios of H_2O and O_4 dSCDs at 3 telescope elevation were converted to H_2O VCDs assuming a lightpath at ground level under normal conditions and a water vapour scale height of $2\,km$ and using the correction factor of 2.6. Qualitatively the latitudinal variation of the *ANT XXVIII/1-2* and GOME-2 data agree. For a quantitative comparison further radiative transfer modelling to obtain tropospheric water vapour profiles from the ship-based data would be needed.' Further comparisons of VCDs are outside the scope of this manuscript. The caption of Fig. 2 already contains the time of the averaged GOME-2A VCDs.

28. p.7, l.1: I0(lambda) is introduced a second time

    Removed this.

29. p.7, l.2: OD is not introduced yet

    Added.

30. p.7, l.3: why only partly?

    Partly was indeed the wrong word here, we reformulated to 'The measured OD of the broad-band extinction and scattering by molecules and particles is represented by a polynomial'

31. Eq (1), (2): please use same symbol for concentration

    Done.

32. Eq (1): add a bracket to indicate the summation; the polynomial p(lambda) is a different one than the one introduced in the line 3 above for the measurements and the cross section here should be a differential cross section

   Formally, we think no brackets are needed here. The polynomial is the same as mentioned in line 3. We added here, following a suggestion from the first reviewer, that we refer here to the total absorption cross-section σ.

33. p.7, l.9: See above; maybe add somewhere before already that MAX-DOAS measures scattered sunlight and LP-DOAS is an active technique.

   We added this at the introduction of the instruments.

34. p.7, l.12: spectral width

   Done.

35. p.7, l.14-15: The sentence about the residual is confusing at this point. Maybe remove?

   We changed 'residual' to 'measurement error of slant column density'. This way we can point out the advantage of the MAX-DOAS measurements without using the word 'residual' in this context.

36. p.8, l.4-6: The total light path is from the institute to the train station and back to the institute?

   Yes. We added that the light also travels back from the retro reflector to the telescope.

37. p.8, l.6: The spectral resolution is redundant information here. Was mentioned before. Section 3.1: I suggest swapping the first 2 paragraphs.

   Swapped the two paragraphs.

38. p.8, l.11: Not the measurement sequence but the correction with the background spectra ensures the independence.

   We split the sentence and added that the measurement spectra are corrected explicitly with the background spectrum.

39. p.8, l.17: high-pass filtered literature cross-sections: aha! That should be mentioned before.

   As this is only the case for the LP-DOAS measurements, this is mentioned here and not at the general DOAS description. The MAX-DOAS data is not filtered and only the polynomial is applied.

40. p.8, l.27: s.a., symbol for concentration.

   s.a., already changed.

41. p.8, l.31: A Fraunhofer spectrum always refers to the extra-terrestrial spectrum of the sun (or another star).

   As it seems to be usual to name the reference spectrum for the MAX-DOAS evaluation Fraunhofer Reference (as also in Platt and Stutz 2006), we added here once 'A so-called Fraunhofer reference spectrum (we follow

the customary nomenclature to call such a spectrum Fraunhofer spectrum although it also contains spectral features from Earth's atmosphere)' and continue to use this name later on in the manuscript. As ground-based MAX-DOAS instruments have no chance to measure an extra-terrestrial spectrum of a star, typically a spectrum with only small absorptions is used as the so-called 'Fraunhofer reference spectrum'. This is often a zenith sky spectrum, as that is typically a spectrum with the smallest amount of atmospheric absorption which can be recorded with the given instrument. As MAX-DOAS instruments are typically not radiometrically calibrated (see e.g. [Wagner et al., 2015] and [Lübcke et al., 2016]), and thus the instrument response function is not perfectly known. Since the solar atlases often still contain telluric absorption lines (compare e.g. the data from [Kurucz et al., 1984] and [Chance and Kurucz, 2010]), it is often better (in terms of minimising the fit residuals) to use a reference spectrum recorded by the same instrument for the spectral retrieval. This is especially important for the detection of weak absorbers.

42. Table 2: What is this Add. Polynomial degree?

The additional polynomial is used in spectral retrievals of MAX-DOAS data to compensate instrumental stray light and usually neglected effects, as e.g. vibrational Raman scattering (VRS, Lampel et al 2015). We added a sentence to the description of the spectral retrieval of MAX-DOAS data: 'An additional intensity offset polynomial was used in the spectral evaluation to compensate for instrumental stray light, as described e.g. in [Peters et al., 2014].' An overview of different implementations can be found in [Peters et al., 2016].

43. p.10, l.1: Fraunhofer: s.a. and another time below as well.

s.a.

44. p.10, l.2: full stop after bracket

Done.

45. p.10, l.3: Remove the last the of the line

Done.

46. p.10, l.6: ANT XXVIII/1-2 or ANT XXVIII? Please unify in manuscript.

Done.

47. p.10, l.16: spectral resolution is redundant information

Removed.

48. p.10, l.20: Why Figure 5 before Figures 3 & 4?

As the LP-DOAS measurements yield direct concentration values along the lightpath with the need to consider radiative transport, it was decided to start with the LP-DOAS measurements instead of the MAX-DOAS observations. Therefore the nicer fits (figure 5) are found after the LP-DOAS data

for the MAX-DOAS data. We added to the introduction of the results, that the LP-DOAS data 'have the advantage of a well-defined light path length' and are therefore presented firstly.

49. p.10, l.21: 40 telescope angle.

Changed.

50. p.10, l.21: Spectra recorded at. . .: why not remove the sentence in l.1-2, p.10 then?

Good idea, done.

51. p.10, l.25: Are those the dSCD measurement errors? Please clarify. Also state that this disregards possible systematic errors.

Added: 'This estimate potentially disregards possible systematic errors, but these are estimated to be small compared to the water vapour absorption ($< 2 \times 10^{-4}$) as the residuals are dominated by random shot noise (see Fig.5)'.

52. p.10, l.26: This section is about the DOAS spectral fitting. So a reference to a linear fit is confusing here. Please add more explanation or move/remove this sentence.

We added '... the residual of the linear fit of H$_2$O/O$_4$ ratios at 363 and 477nm shown in ...'.

53. p.11, l.25: OD; s.a.

Explanation added above.

54. p.11, l.28-30: Please elaborate or state reference.

First of all we added a small introduction to this paragraph (with references) in order to introduce the Ring effect itself: 'The Ring spectrum itself compensates the measured apparent optical density due to inelastic scattering of sunlight at air molecules [Shefov, 1959, Grainger and Ring, 1962], which leads to an effective filling-in of Fraunhofer lines in the measured spectrum of scattered sunlight e.g. [Wagner et al., 2009] and references therein.'

Further elaboration such as RTM for the effective temperature of the Ring effect would be out of the scope of this work. We added an estimate of the total magnitude of this effect:'For a Ring signal of 2.5×10^{25} molec cm^{-2} (which is typical for MAX-DOAS observations), the temperature dependence of the Ring effect results in an OD of 5×10^{-4} for a temperature difference of 30 K. In our analyses warmer effective Ring temperatures were found at low telescope elevation angles.' We did also run the evaluations again without correction of the Ring temperature effect and found no significant changes of the overall result regarding the size of the water vapour absorption around 363nm. It led however to elevation angle separated systematic residual structures as found by PCA analysis (similar to [Lübcke et al., 2016]) of the resulting fit residual spectra and was therefore included in the final analysis.

55. p.12, l.3: when co-adding spectra from more than

Modified.

56. p.12, l.12: Remove paragraph break.

   Done.

57. p.12, l.16: Is the stated time period different from the one in Table 1?

   Only a subset of the measurements was used. During other days, e.g. the short-cut measurements failed. Therefore we reduced the dataset to those measurements where optimal conditions were found. We added 'when optimal instrumental performance could be guaranteed'

58. p.12, l.20: Are you really losing 15 min for each hour? Please clarify.

   No, background measurements are performed for lamp reference measurements as well as for atmospheric measurements, which means that four spectra are recorded during each sequence. We added to the paragraph about the background correction, that these are four spectra in total. The time to change the wavelength range is negligible in this configuration and these exposure times.

59. p.12, l.25: The data in Figure 3 does not support this statement. Also, this is the only time Figure 3 is mentioned in the text of the manuscript (besides in the caption for Figure 2, but Figure 2 is barely mentioned either. Those would be candidates for removing in order to shorten the manuscript.).

   Adding more spectra was tested, but did not yield satisfying results or improved the results. Longer times for co-adding spectra increases also the effect of potential instrumental changes. We decided to keep the figures to show the results of the LP-DOAS measurements.

60. p.12, l.29: 20% is not low humidity?

   This is not necessarily low absolute humidity during summer, compared to the overall data set. These values were observed around noon with high outside temperatures.

61. p.13, l.2: Maybe remove the uncertainty estimate at this point since it has just been stated in the line above and the actual interesting number is 0.7 and not 0.05.

   done

62. Figure 4, caption: 2.31? The text states 2.4. The right panel of the figure is not mentioned in the text at all.

   2.31 is the factor when allowing an y-axis intercept in the fit, 2.39 when no y-axis intercept is allowed for. This is already stated in the text. The right panel is now mentioned explicitly.

63. p.14, l.1-3: Please rephrase.

   Sentence split and modified: 'These fitting intervals were selected in a way, that the wavelength of the main absorptions of O_4 and H_2O are at similar wavelengths. This needs to be done in order to have approximately the same radiative transfer properties for both absorbers'

64. p.14, l.10: The figure states R2 = 0.74 for both cases. Please clarify!

Thanks for pointing this out. We checked the script and updated the plot. The wrong variable was written to the plot, but the correct data is found in the output for the table of results using different O4 XS.

65. Figure 6, caption: There is only 1 error bar and that is attached to the linear fit. Does it refer to the error bars of the measurements though? Please clarify!

The errorbar represents the mean measurement error for all considered measurements, it is now further clarified in the caption.

66. For the green box in the top right panel, how are the measurement uncertainties combined? The figures say O4 at 476nm and not 477 as in the caption.

We replotted the figure using consistent wavelengths. The green box represents twice the mean DOAS fit error for the measurements as stated in the caption of the figure.

67. p.17, l.5-7: I dont understand this paragraph. Worse in comparison to what? Did you state the number of the combined correlation somewhere? 0.91 is a pretty good correlation.

Worse in comparison to the correlation of their respective ratios. Added 'compared to the correlation of their respective ratios'

68. p.17, l.8-11: This information should already be stated on p.14,l.9-10. Also maybe mention somewhere that this is the reason for the different numbers for n in Table 3.

Moved. We added 'These conditions lead to different numbers of valid observations in Table 3 for different spectral retrieval settings'.

69. p.17, l.14: see also Table 3

changed

70. p.17, l.16: latitudinal s.a.

removed here.

71. p.18, l.16: includes more measurements: see comment above

See comment above.

72. p.18, l.31: could not be identified for either of the two line lists or cruises? Please clarify!

This was tested for M91. We added this. *ANT XXVIII/1-2* data was also analysed, but not included in the manuscript in this case as it did not yield further information and larger detection limits.

73. Figure 7, caption: add space after DMS

Done.

74. p.19, l.12: an RMS

Changed.

75. p.19, l.15: than in either the BT2 or the HITEMP

changed to 'to be better predicted in the *POKAZATEL* line list than in the BT2 and the HITEMP line list'

76. p.19, l.15-18: This information should have been in the intro.

Shortened the sentence here and added to the introduction.

77. Figure 8: gridlines would be helpful in this figure.

We added gridlines to this figure.

78. p.22, l.18: 3 elevation angle

Added

79. p.22, l.16: polynomials with degrees 0-2 were applied in order to test. . .

Changed. We added also '... to estimate the dependence of the inferred upper limits on the degree of the DOAS polynomial. The polynomial could compensate for water vapour absorption if it would be a rather broad absorption in this spectral region as suggested by [Du et al., 2013]'

80. Table 4: Last sentence of the caption seems to be quite important, however, is not explained in the text.

This sentence was moved from the caption to the text.

81. Section 4.9, title: Please add that you investigate the accuracy of the wavelength calibration here

Modified to 'Estimation of the accuracy of the shape and wavelength calibration of the POKAZATEL H$_2$O cross-section' (see above)

82. p.23, l.7: why is there an R introduced for the residual spectra? Its not used anywhere else.

Removed.

83. p.24, l.5: Within 0.1 cm-1 in comparison to what?

Compared to laboratory measurements. We added 'from measured data from [Maksyutenko et al., 2007]'

84. p.25, l.1: Section title is misleading. This section only refers to the visible range.

Added 'in the blue wavelength range'. This is important, as these were used as a 'reference' to compare to the UV data.

85. p.25, l.5: . . . magnitude of the water vapour. . . blue wavelength range. . .

We restructured this sentence to 'The uncertainty of the absolute magnitude of the water vapour cross-section (HITEMP) in the blue wavelength from 452-499 nm is less than 15%: ...'.

86. p.25, l.5-8: Where does this information come from?

We added 'when fitting the absorption bands separately analogously to [Lampel et al., 2015]' to the end of the sentence.

87. P.25, l.14: formatting issue H2O-dSCD

    Fixed.

88. p.25, l.21-23: Please split sentence

    Split sentence and removed one of the 'which'.

89. p.25, l.27-29: Please split sentence

    Done.

90. p.25, l.30-31: No direct correlation. . . I dont understand this. Please elaborate.

    We meant 'No correlation of the water vapour dSCDs at 363 nm with the square term of the O_4 absorption was found for the *ANT XXVIII/1-2* dataset.' This is now corrected

91. p.26, l.1-3: Maybe use the term water vapour contamination here.

    Good idea, changed.

92. p.27, l.2: formatting issues for references

    Fixed.

93. p.27, l.4: formatting issues for reference

    Fixed.

94. p.27, l.20: section 1.2 does not mention the correction factor

    Removed.

95. p.27, l.30: formatting issues for reference and brackets

    Fixed.

96. p.28, l.5-8: Why didnt you perform this analysis separately then for cases with and without HONO?

    The HONO absorptions are close to the detection limit, which make a simple filtering difficult or impossible. We tried to filter based on the NO2 dSCDs, but as large NO2 dSCDs introduce again residual structures, these would have to be filtered out as well. Finally such a pre-filtered data set would have looked a bit arbitrarily filtered. Therefore we used the complete dataset using only the RMS as quality indicator. The positive value of the mean HONO dSCD is however in agreement with zero, it is within the standard deviation of the observed values $(1.0 \pm 2.3) \times 10^{14}$ molec cm^{-2} . We added to the manuscript '... , but it is in agreement with zero within the standard deviation of the observed values. Filtering the results based on HONO dSCDs could have introduced a negative bias, as the observed HONO values are generally close to the respective detection limits. We therefore used the complete MAX-DOAS data set.'

    Furthermore we added 'Only fit results with an initial RMS of the fit residual of less than 4×10^{-4} were considered' to the introduction of this subsection.

97. p.29, l.1: alternative to what?

Alternative to the standard evaluations, which are described in ([Bobrowski et al., 2010, Hörmann et al., 2013]). However, we removed 'alternative' .

98. p.29, l.7: remove itself

Removed.

99. p.29, l.16: rephrase sentence

'in the blue spectral'→' in the blue spectral range'

100. p.29, l.22: Maybe join these two sections?

We prefer to keep the sections separated, as one involves the detection of water vapour absorption in the UV, while the other is an addition to [Lampel et al., 2015].

101. Figure 11, caption: different bands listed in Table6; use unity instead of 1.

Changed.

102. Table 6, caption: relative integrated absorption values: relative to what? Please elaborate;

'relative integrated absorption values' → 'integrated absorption values relative to W3'

103. The second to last, not last row shows the scaled HITEMP data.

The last row was removed in the final version of the manuscript, but not from the caption of the table. We removed it also there.

104. p.31, l.10: Who are they?

changed to 'these'.

105. Table 7, caption: formatting issues with reference

Changed.

106. Appendix: Why are table 7 and 8 in an appendix? Then the text discussing those should also be moved to the appendix.

We moved both tables to the part of the text which discusses these results.

107. Table 8: Im not sure what is done here. What are the relative DOAS fit errors? There is no Window 5 in here.

These two tables are added in analogy to [Lampel et al., 2015], as extension of those. It uses the same MAX-DOAS datasets, but POKAZATEL was not available back then.

More general comments:

108. More general comments: * The abstract doesnt list anything about the O4 studies or the failed identification of other water vapour lines in the UV

We added that different O$_4$ absorption cross-sections were tested: 'The results were independent of the used literature absorption cross-section of O$_4$, which overlays this water vapour absorption band'

109. More general comments: * References to dissertations cannot be accessed if no link is provided.

We added a URL in both cases.

References

[Bobrowski et al., 2010] Bobrowski, N., Kern, C., Platt, U., Hörmann, C., and Wagner, T. (2010). Novel so$_2$ spectral evaluation scheme using the 360-390 nm wavelength range. *Atmospheric Measurement Techniques*, 3(4):879–891.

[Chance and Kurucz, 2010] Chance, K. and Kurucz, R. (2010). An improved high-resolution solar reference spectrum for earth's atmosphere measurements in the ultraviolet, visible, and near infrared. *Journal of Quantitative Spectroscopy and Radiative Transfer*, 111(9):1289 – 1295. Special Issue Dedicated to Laurence S. Rothman on the Occasion of his 70th Birthday.

[Du et al., 2013] Du, J., Huang, L., Min, Q., and Zhu, L. (2013). The influence of water vapor absorption in the 290-350nm region on solar radiance: Laboratory studies and model simulation. *Geophysical Research Letters*, 40(17):4788–4792.

[Grainger and Ring, 1962] Grainger, J. and Ring, J. (1962). Anomalous fraunhofer line profiles. *Nature*, 193:762.

[Hörmann et al., 2013] Hörmann, C., Sihler, H., Bobrowski, N., Beirle, S., Penning de Vries, M., Platt, U., and Wagner, T. (2013). Systematic investigation of bromine monoxide in volcanic plumes from space by using the gome-2 instrument. *Atmospheric Chemistry and Physics*, 13(9):4749–4781.

[Kurucz et al., 1984] Kurucz, R. L., Furenlid, I., Brault, J., and Testerman, L. (1984). *Solar Flux Atlas from 296 to 1300 nm*. National Solar Observatry, Sunspot, New Mexico, U.S.A.

[Lampel et al., 2015] Lampel, J., Pöhler, D., Tschritter, J., Frieß, U., and Platt, U. (2015). On the relative absorption strengths of water vapour in the blue wavelength range. *Atmospheric Measurement Techniques*, 8(10):4329–4346.

[Lübcke et al., 2016] Lübcke, P., Lampel, J., Arellano, S., Bobrowski, N., Dinger, F., Galle, B., Garzón, G., Hidalgo, S., Chacón Ortiz, Z., Vogel, L., Warnach, S., and Platt, U. (2016). Retrieval of absolute so$_2$ column amounts from scattered-light spectra – implications for the evaluation of data from automated doas networks. *Atmospheric Measurement Techniques Discussions*, 2016:1–33.

[Maksyutenko et al., 2007] Maksyutenko, P., Muenter, J. S., Zobov, N. F., Shirin, S. V., Polyansky, O. L., Rizzo, T. R., and Boyarkin, O. V. (2007). Approaching the full set of energy levels of water. *Journal of Chemical Physics*, 126(24):241101–241101.

[Peters et al., 2016] Peters, E., Pinardi, G., Bosch, T., Richter, A., Wittrock, F., Seyler, A., Burrows, J. P., Roozendael, M. V., Hendrick, F., Drosoglou, T., Bais, A., Kanaya, Y., Zhao, X., Strong, K., Lampel, J., Frieß, U., Volkamer, R., Koenig, T., Ortega, I., Dix, B. K., Piters, A., Puentedura, O., Navarro, M., Gomez, L., Gonzalez, M. Y., Remmers, J., Wang0, Y., Wagner, T., Wang, S., Saiz, A., Nieto, D. G., Cuevas, C. A., Querel, R., Johnston, P., Postylyakov, O., Borovski, A., Bruchkouski, I., Li, C., Hong, Q., Rivera, C., Grutter, M., Stremme, W., Khokhar, F., , and Khayyam, J. (2016). Investigating differences in doas retrieval codes using mad-cat campaign data. *Atmospheric Measurement Techniques Discussions, prepared for publication*.

[Peters et al., 2014] Peters, E., Wittrock, F., Richter, A., Alvarado, L. M. A., Rozanov, V. V., and Burrows, J. P. (2014). Liquid water absorption and scattering effects in doas retrievals over oceans. *Atmospheric Measurement Techniques*, 7(12):4203–4221.

[Shefov, 1959] Shefov, N. N. (1959). Intensivnosti nokotorykh emissiy sumerochnogo i nochnogo neba (intensities of some emissions of the twilight and night sky). *Spectral, electrophotometrical and radar researches of aurorae and airglow, IGY program, section IV*, 1:25.

[Wagner et al., 2015] Wagner, T., Beirle, S., Dörner, S., Penning de Vries, M., Remmers, J., Rozanov, A., and Shaiganfar, R. (2015). A new method for the absolute radiance calibration for uv-vis measurements of scattered sunlight. *Atmospheric Measurement Techniques*, 8(10):4265–4280.

[Wagner et al., 2009] Wagner, T., Deutschmann, T., and Platt, U. (2009). Determination of aerosol properties from MAX-DOAS observations of the Ring effect. *Atmospheric Measurement Techniques*, 2(2):495–512.